Modeling Central Pattern Generators in Sand Crabs

By

Alexander Fraser Cooper Hodge

B.Sc., University of Victoria, 2000

A Thesis Submitted in Partial Fulfillment of the
Requirements for the Degree of
MASTER OF SCIENCE
in the Department of Mathematics and Statistics

We accept this thesis as conforming
to the required standard

Dr. R. Edwards, Department of Mathematics & Statistics, University of Victoria

Dr. P. van den Driessche, Department of Mathematics & Statistics, University of Victoria

Dr. D. H. Paul, Department of Biology, University of Victoria

Dr. G. de Vries, Department of Mathematical and Statistical Sciences, University of Alberta

Supervisors: Dr. R. Edwards and Dr. P. van den Driessche

Abstract

Ordinary differential equation models based on those of Hodgkin and Huxley are presented in an effort to describe a particular anomalous digging behaviour in the anomuran decapod crustacean *Emerita analoga*. At the onset of a dig, the fourth (hindmost) right and left legs stroke together about half a cycle out of phase with the uropods (last abdominal appendages). During digging, however, the phase relationships between the fourth legs and uropods change and one leg (either left or right) begins to lead the other. Two general approaches are taken here to model the central pattern generators (CPGs) that coordinate each appendage, and these CPG models are coupled together in order to describe the full network. First, CPGs comprise cells, or small groups of cells described by Morris-Lecar equations. Simply coupling these cellular models together results in high dimensional systems of ordinary differential equations that can only be analysed numerically except in special symmetric cases. However, using similar equations to model each CPG permits averaging which reduces the "important" dimension of the system to three, namely a single phase variable for each appendage. So the second approach taken here is to model each CPG as a single oscillator coupled to others by a phase response function, computed numerically from the cellular differential equations. The resulting three dimensional system is much easier to analyse and it is used to show that with minimal sensory input, a neural network consisting of three coupled oscillators is sufficient to account for the anomalous digging behaviour in *Emerita*.

Examiners:

[redacted]

Dr. R. Edwards, Department of Mathematics and Statistics, University of Victoria

[redacted]

Dr. P. van den Driessche, Department of Mathematics and Statistics, University of Victoria

[redacted]

Dr. D. H. Paul, Department of Biology, University of Victoria

[redacted]

Dr. G. de Vries, Department of Mathematical and Statistical Sciences, University of Alberta

Table of Contents

List of Tables

List of Figures

Acknowledgements

Thank you Rod, Pauline, and Dorothy. Without your knowledge, support encouragement and direction, I'd still be trying to define the problem.

Also, thanks to all of my family and friends for providing timely and necessary distractions.

Victoria, British Columbia
March, 2003

Alex Hodge

To All the Crustaceans

Chapter 1

Introduction

This work was motivated by observations made by Dr. D. H. Paul and Dr. Z. Faulkes of an anomalous digging behaviour by the sand crab *Emerita analoga*. Ensuing discussion between Dr. Paul and Dr. R. Edwards spawned the idea that perhaps, since so little is known about the actual neurophysiology of *Emerita*, mathematical models could help suggest some potential neural arrangements that could yield the notable behaviour, namely an unusual phase relationship between the fourth pair of legs and the uropods.

It is supposed [3] [4] [5] that each appendage involved in digging is controlled by a small cluster of neurons called a central pattern generator (CPG). The behaviour of the CPGs together with the nature of the coupling between them results in the motor output. In the following, models will be presented to describe both the CPGs themselves and the ways they can be coupled. The goal is to be able to use these models to elucidate the neural mechanisms responsible for the observed behaviour, thus simplifying the search for the actual neurons.

In this chapter and in Chapter 2, some relevant background material will be

presented. In Chapter 3, the first network will be proposed, consisting of three Morris-Lecar neurons. The resulting system of ordinary differential equations (ODEs) will be reduced in Chapter 4, using known averaging techniques, to a 3-dimensional system for analysis. Chapter 5 contains descriptions of more elaborate, higher dimensional models for each CPG along with their numerical solutions and reduction to phase equations.

The reduction of the network of 3 m-dimensional oscillators to a system of phase equations is the main focus of this work.

1.1 Description of *Emerita analoga*

The sand crab (or mole crab) *Emerita analoga* is an anomuran decapod crustacean [3] [26], inhabiting the surf zone on large sandy beaches. The segmented body plan of *Emerita* is, of course, similar to that of other crustaceans such as crayfish as well as other anomurans like the familiar hermit-crabs or porcelain crabs, but *Emerita*'s appendages are adapted for digging and swimming [3] rather than for walking. Figure 1.1 shows *Emerita* just above the bottom, having just emerged from the sand. Figure 1.2 shows a lateral schematic clearly illustrating *Emerita*'s four pairs of legs and a pair of uropods (the posteriormost appendages). When the organism digs, each of its legs follows a coordinated trajectory [3] [5] as illustrated in Figure 1.2. Note in the figure that the first pair of legs is not used in digging. During a dig, the second and third pairs of legs cycle in a direction opposite to that of the fourth (posteriormost) pair, suggesting that the control centres responsible for their movements are separate [3] [5].

Each of *Emerita*'s thoracic segments bears a pair of legs controlled mostly by the

Figure 1.1: Photograph of *Emerita analoga* showing three pairs of digging legs and the pair of uropods (top)(Reproduced with the permission of Dr. D.H.Paul).

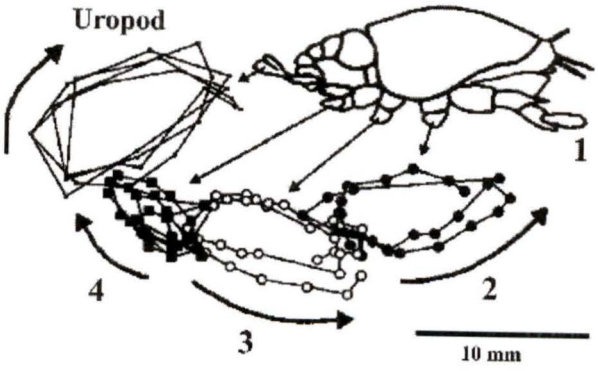

Figure 1.2: Schematic of the trajectories of tips of the digging legs and uropods [3] (Reproduced with the permission of Dr. D.H.Paul).

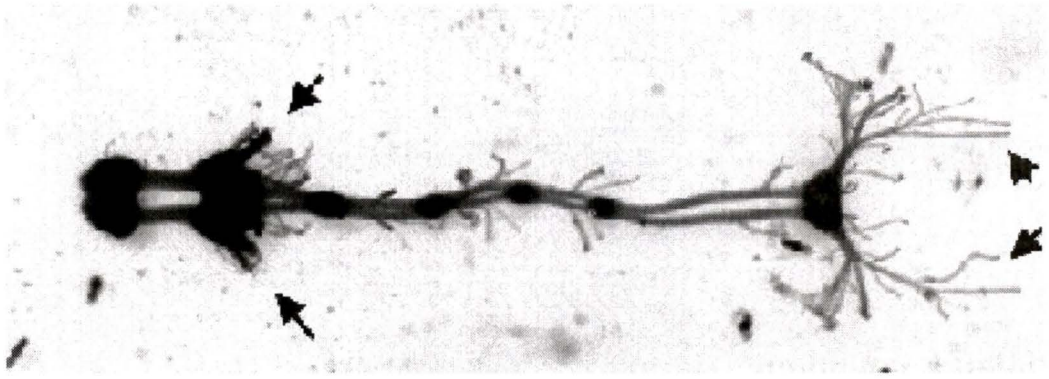

Figure 1.3: Isolated posterior portion of the CNS from *E. analoga*. The locations of the 4^{th} leg CPGs (left arrows) and the uropod motor nerves (right arrows) are indicated. (Reproduced with the permission of Dr. D.H. Paul

local ganglion [3] [4] [5]. Figure 1.3 shows a portion of *Emerita*'s central nervous system (CNS) in order to illustrate the location of the neurons responsible for leg and uropod movement. The arrows on the left indicate the fourth thoracic ganglion and those on the right point to motor nerves for controlling the uropods. Note that the ganglia are separated spatially.

When *Emerita* initiates a dig, the 4^{th} legs behave in bilateral synchrony, whereas the right and left legs on the second and third segments alternate. However, when digging, the posteriormost pair of legs show the ability to operate somewhat independently. As the dig progresses, the cycling of the fourth legs becomes asymmetric — a behaviour not observed in other related crustaceans.

1.2 Behaviour and Data to be Modelled

The behaviour to be modelled is precisely this anomalous rhythmic cycling of the uropods and 4th pair of legs in *Emerita* during digging. At the beginning of a dig, the right and left legs beat together, about half a cycle out of phase with the uropods.

Figure 1.4(a) shows two separate EMG recordings (A and B). The shaded regions in the latter depict substantially different phase relationships between the posterior appendages. As the dig progresses, the relative phases of the two legs change, and one starts to lead the other. By the end of the dig, the left leg, right leg, and pair of uropods can be cycling all about $\frac{1}{3}$ of a cycle out of phase with each other as indicated in Figure 1.4(b) [3] [4] [5] [23] [25]. Additionally, the frequency of cycling diminishes by a factor of about 2 throughout the dig.

Essentially, the purpose of this project is to propose a mathematical model that can describe *Emerita's* digging behaviour, and satisfy the following observations:

- For every cycle of the right leg (R4) there is exactly one cycle of the left leg (L4) and one cycle of the uropods.
- The mean activation time between the right and left legs remains roughly half a cycle out of phase with the uropod.
- No leg ever cycles in phase with the uropods.
- The phase differences between the right and left hindmost legs can range roughly between 0 and $\frac{2\pi}{3}$ throughout a dig.
- Either left or right leg can lead.
- The frequency of the oscillations diminishes as the dig progresses.

Because it is not seen in closely related organisms, perhaps the most interesting aspect of *Emerita's* behaviour (and the motivation for this work) is the ability of its right and left hind legs to operate independently of the other legs, and that their rhythmic movements appear to be coordinated with uropod movements.

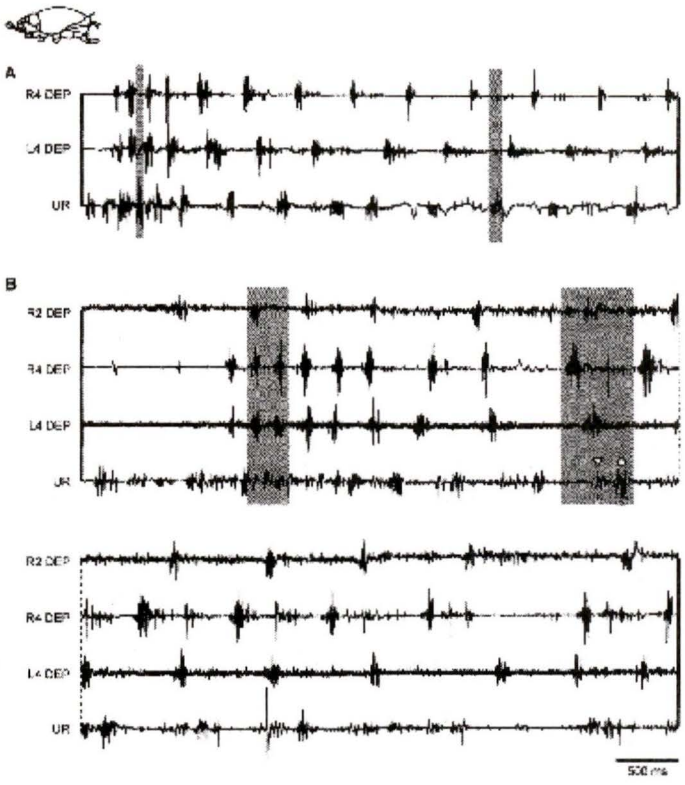

(a) Electromyogram recordings from second legs, fourth legs, and uropods obtained by Dr. D.H.Paul and by Dr. Z.Faulkes The phase relationships of the appendages differ in the two shaded regions.

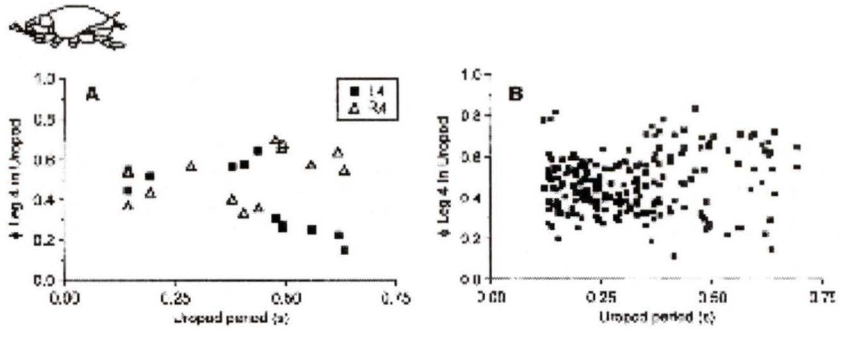

(b) Phase vs. time [3]. The relative phases of the legs and uropods stray from near 0.5 as the dig progresses

Figure 1.4: Depiction of digging behaviour (Reproduced with the permission of Dr. D.H.Paul)

1.3 Pattern Generating Circuits

A Central Pattern Generator (CPG) is a small group of neurons that interact to produce a rhythmic output that each neuron might not be capable of alone. They are particularly useful in modelling when the dynamics of each neuron are far less important than the collective dynamics of the local system [21]. A CPG can be considered a "black box" comprising many components, whose behaviour can be described by relatively few equations. In many cases, behaviour of a complex interaction of many neurons can be inferred from an understanding of the behaviour of a small system of interacting CPGs [22] [25].

In *Emerita*, each appendage is likely driven by its own CPG, comprising on the order of 30–70 neurons, located in the CNS [3] [4] depicted in Figure 1.3. The repetitive beating, or cycling of the legs and uropods suggests that, at least in the crudest sense, each of the CPGs should be considered some sort of arbitrary oscillator. The nature and complexity of each, together with the nature of the coupling between them, dictates the behaviour of the complete network.

For the sake of illustrating some notation and figure conventions, Figure 1.5 shows some of the ways in which arbitrary identical oscillators can influence each other depending on their coupling. Each oscillator is represented by a circle and lines joining oscillators denote coupling. In Figure 1.5(a) a single oscillator is shown together with a periodic solution of one of its variables (found numerically). In Figure 1.5(b), (c), and (d), two such oscillators are shown with variations on coupling. The graphs on the right depict numerical solutions to the analogous variable in each oscillator. When there is no coupling (b) the oscillators tend to their own limit cycles and the phase difference between them depends only on the initial conditions. When coupling

between them is inhibitory (indicated by the filled circles in (c)) the oscillators tend to a limit cycle in which they are exactly half a cycle out of phase with each other. Conversely, when coupling is excitatory (indicated by the hollow triangles in (d)) there exists a stable limit cycle in which the oscillators are locked with the same phase.

In Figure 1.5(e), three oscillators are coupled by inhibitory terms, and the system tends to a solution where all three cycle with phase differences of $\frac{2\pi}{3}$ radians. Finally, in Figure 1.5(f) there is no bilateral coupling and the network tends to a solution where two oscillators are together and out of phase with the third. Of course it is important to note that this serves just as an illustration and will be discussed in more detail later. The necessary observation is that various simple arrangements of oscillators can behave very differently, depending only on their coupling.

Since so little is known about the actual neural arrangements in *Emerita*, assignment of a particular oscillator to describe their CPGs is somewhat arbitrary, and is limited only loosely by "what seems reasonable". The selection of equations is motivated by previous work on other crustaceans [20] [28] [29] [30] [31], and is restricted to equations specifically intended to describe neural dynamics.

The arrangement of CPGs in Figure 1.5(f) has an output pattern that could represent the phase relationship between the fourth legs and uropods in the early part of a dig. Likewise, the three oscillators cycling with phase differences of $\frac{2\pi}{3}$ depicted in Figure 1.5(e) is similar to the cycling of the sand crab's appendages near the end of a dig. This suggests the hypothesis that intermediate arrangements could produce intermediate behaviour, and thus describe the dig.

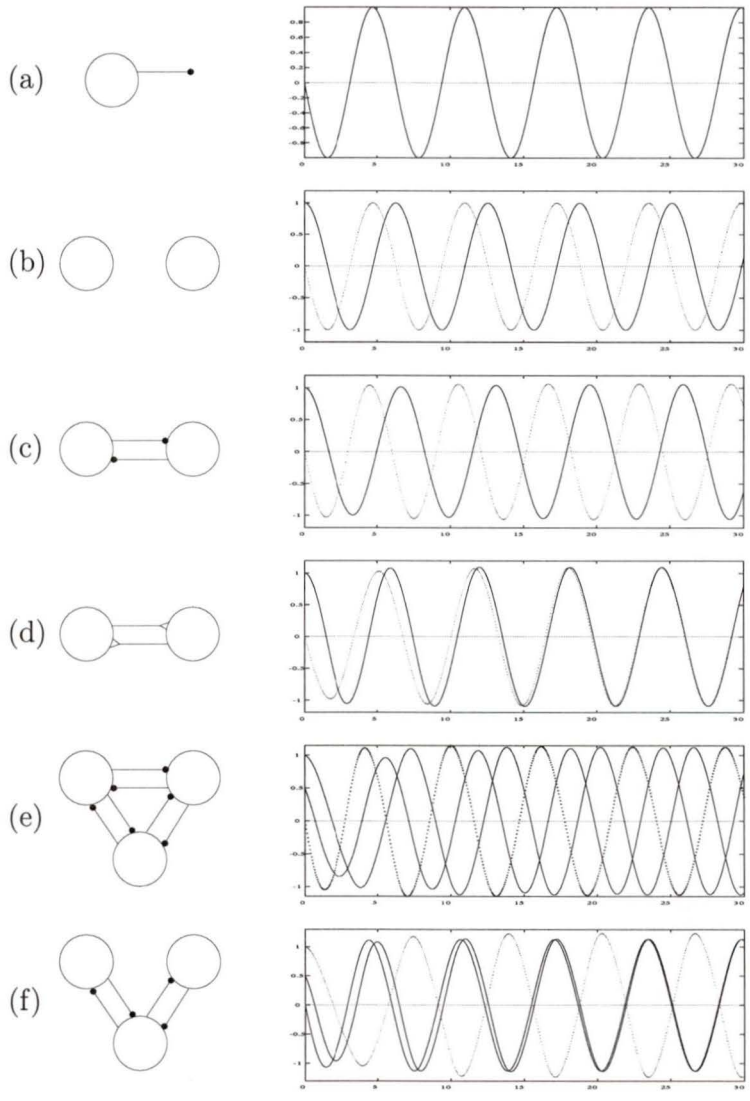

Figure 1.5: Some possible results of coupling oscillators. The filled circles represent inhibitory connections and the hollow triangles represent excitatory connections. The transient behaviour in (c)-(f) indicates that the oscillators tend to stable phase relationships.

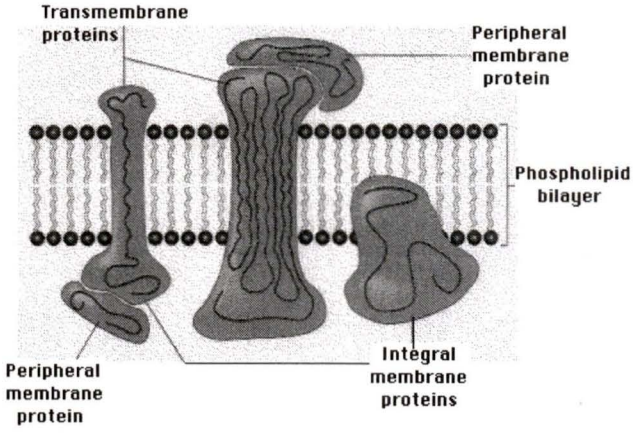

Figure 1.6: Cross-section of a neural membrane with embedded proteins.

1.4 Brief Description of Cell Membrane

The cell membrane is a very complicated structure that will not be discussed in much detail here. However, it is prudent to outline the aspects of the membrane that are relevant to models describing its electrical properties. Figure 1.6 shows a cross-section of cell membrane with "important" features indicated.

The main structure is the phospholipid bilayer. Phospholipids are large bipolar molecules that can arrange themselves into energetically favourable layers in polar solutions (like water). In these arrangements, the polar ends are in contact with the solution and the non-polar ends are in contact with each other forming the base of the cell membrane [15].

The phospholipid bilayer forms a barrier to molecules (especially ions) dissolved in the solutions, since they cannot readily diffuse across its middle (non-polar) region. However, many transmembrane proteins (labelled in the figure), sometimes called channel proteins, have evolved to shuttle these solutes across. A host of channel proteins have been identified, and most are very specific to the molecules they

transport [15].

Unlike conventional current (electron flow), the currents across cell membranes are due mainly to ion movement. For the purpose of this project, it is sufficient to assume that a neural membrane consists of a phospholipid bilayer with embedded populations of any of the three major (Sodium (Na), Calcium (Ca) and Potassium (K)) channels. An important property is that each channel can comprise several gates, all of which must be open in order for ions to pass.

1.5 The Model Assumptions

Since so little is known about the neural structures responsible for digging in *Emerita*, it is necessary to make both physiological and mathematical assumptions before trying to model the behaviour. The crayfish, a related organism, has been studied much more extensively (see, for example, [21] [23] [25] [29] [30]), so inferences will be based on the known structures of crayfish ganglia. Some necessary assumptions are:

- *Emerita*'s CNS is similar to the crayfish CNS.
- Spiking interneurons transmit signals between spatially distinct CPGs.
- Non-spiking interneurons transmit signals within CPGs.
- The Morris-Lecar equations give a reasonable description of non-spiking neurons.
- The Hodgkin-Huxley or the FitzHugh-Nagumo equations give a reasonable description of spiking neurons.

- The effect of coupling between neurons is weak compared to the intrinsic properties of the neurons.

With these assumptions, it is possible to construct models of the entire network based on existing models of the components.

Chapter 2

Description of Model Equations

Two natural tendencies in modelling are to describe a system in as much detail as possible in order to obtain a very accurate model, or to propose the simplest possible model that can account for specific observations. In modelling the digging behaviour in *Emerita*, both of these approaches will be applied in different descriptions of the CPG's.

Attempting to account for likely detail, existing models describing cellular dynamics will be coupled together in Chapter 3 and 5 to model CPG's, which will, in turn be coupled into a small network whose behaviour mimics that of *Emerita*'s ganglia during digging. Conversely, attempting to simplify in Chapters 4 and 5, each CPG will be modelled by a single ordinary differential equation (ODE) describing its phase along its limit cycle. Of course, the relationships between the detailed cellular models and the abstract phase models will be emphasized, and the two approaches will be shown to yield consistent results.

The dynamics of a single cell can be described by a system of ODEs defined on $\mathbb{R}^n$ (each cell is considered as an n-dimensional oscillator). Hence, a CPG comprising

m cells is at least mn-dimensional. Therefore, a network of k CPGs is at least kmn-dimensional, and likely more since connections between cells can require additional differential equations (DEs), further increasing the dimension of the network.

In a more abstract approach, each CPG is considered as some arbitrary oscillator with a stable limit cycle. So, on reduction, the behaviour of a CPG described formerly on $\mathbb{R}^{mn}$ can be described simply on the circle $\mathbb{S}^1$ by a DE describing its phase along its limit cycle. So the network of k CPGs is described by equations on $\mathbb{T}^k = \mathbb{S}^1 \times \mathbb{S}^1 \times \cdots \times \mathbb{S}^1$, k times.

It is clear that there exist advantages to both approaches, and that there is some tradeoff in the selection of the appropriate models. Using detailed models makes analysis very difficult, but using abstract models increases the likelihood of missing important behaviours. Here the approach will be to construct a cellular model, and treat it analytically as far as possible, and then reduce it to a phase model (using averaging techniques) for further analysis. Numerical solutions will be generated where appropriate to show agreement between cellular and phase models.

The components to be used in the construction of the various models are

- Equations describing excitable membranes (single cells) on $\mathbb{R}^n$.
- Equations describing connections between cells.
- Equations describing k arbitrary oscillator CPGs on $\mathbb{T}^k$.

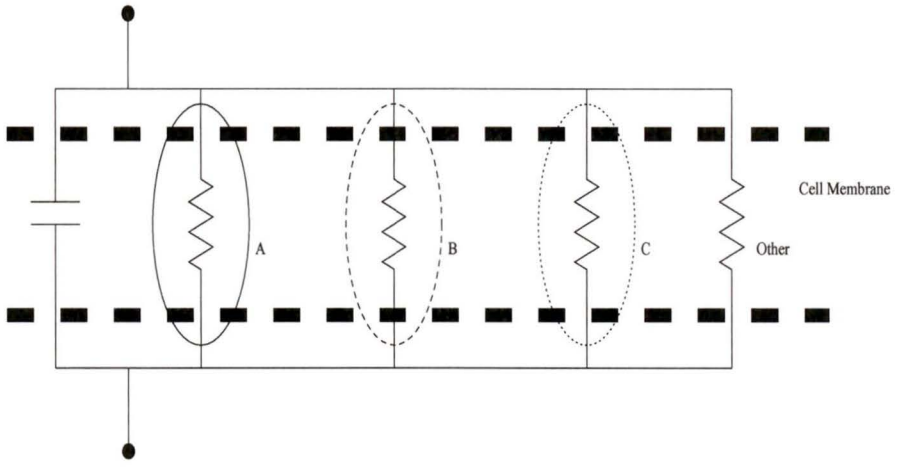

Figure 2.1: Schematic cross-section of a Cell Membrane. The dashed lines represent the phospholipid heads and A, B, and C are channel proteins. Superimposed is a circuit diagram used to develop the $\frac{dv}{dt}$ equation

2.1 Equations Describing Excitable Membranes on $\mathbb{R}^n$

Many attempts to describe the dynamics of neural membranes have been proposed based on the pivotal model by Hodgkin and Huxley [12] [16]. Each of these uses Kirchoff's current law to develop an autonomous nonlinear system of ordinary differential equations that describe how the ionic current flow across a patch of cell membrane can give rise to realistic voltage dynamics. The components of the equations are depicted in Figure 2.1 showing a schematic cross-section of a cell membrane with trans-membrane ion channels. The super-imposed circuit diagram is used in the development of a voltage equation using Kirchoff's Current Law.

To summarize, locally a cell membrane is like a parallel plate capacitor over which the current flow is given by $C\frac{dv}{dt}$, where v is the potential difference across the membrane, t is time, and the parameter C is the capacitance of the membrane. The

current across the membrane can either flow through channels specific to each ion species, or it can "leak" across. So the DE

$$C\frac{dv}{dt} = i_{other} + \sum i_{ionic} \tag{2.1.1}$$

where i_{other} applies to leak and applied currents and i_{ionic} represents current due to ion flow through channels, has a solution $v(t)$ describing the potential difference across a patch of membrane as a function of time. Specifically, the equation

$$C\frac{dv}{dt} = i_A + i_B + i_C + i_{other} \tag{2.1.2}$$

is derived from the circuit diagram in Figure 2.1.

Usually, these models comprise one variable to represent the potential difference across a patch of cell membrane, and one to represent the dynamics of each species of ion, or other current flow. The number of ion species involved (at least as dynamic variables) together with the number of gates per channel and the voltage equation determines the dimension of the system. For example, Hodgkin and Huxley [12] [16] modelled the action potential of the squid giant axon using sodium and potassium channels (now known to comprise sodium activation, sodium inactivation, and potassium gates), yielding a system of equations on $\mathbb{R}^4$. Subsequently, others have proposed simpler models either involving simpler neurons or simpler equations. Morris and Lecar use a two-dimensional model to describe the dynamics of a barnacle muscle fibre, and FitzHugh and Nagumo use a two-dimensional polynomial system to approximate the behaviour of the Hodgkin-Huxley system.

2.1.1 The Hodgkin-Huxley Equations

Hodgkin and Huxley used data collected from voltage clamp experiments on the squid giant axon to deduce the first of these models (on $\mathbb{R}^4$). The predominant channels in

the axon they were studying are sodium (Na) and potassium (K), so Kirchoff's law gives the equation

$$C\frac{dv}{dt} = i_l + i_K + i_{Na} + i \tag{2.1.3}$$

where each term on the right describes a specific contribution to the total current flowing across the membrane. The sodium and potassium channels have nonlinear voltage dependence, and their dynamics are described by additional equations. The full Hodgkin-Huxley system of equations describing the voltage fluctuation and the nonlinear dependence of each ion conductance on voltage is

$$\begin{aligned} C\frac{dv}{dt} &= g_l(v_l - v) + g_K n^4(v_K - v) + g_{Na} m^3 h(v_{Na} - v) + i \\ \tau_n(v)\frac{dn}{dt} &= n_\infty(v) - n \\ \tau_m(v)\frac{dm}{dt} &= m_\infty(v) - m \\ \tau_h(v)\frac{dh}{dt} &= h_\infty(v) - h \end{aligned} \tag{2.1.4}$$

where the functions

$$\tau_k(v) = \frac{1}{\alpha_k(v) + \beta_k(v)} \qquad \text{and} \qquad k_\infty(v) = \frac{\alpha_k(v)}{\alpha_k(v) + \beta_k(v)}$$

are determined qualitatively to fit the data. Here, $k = n, m$, or h and parameters are as defined in Table 2.1. The specific functions used by Hodgkin and Huxley are

$$\begin{aligned} \alpha_m &= 0.1\frac{25 - v}{e^{\frac{25-v}{10}} - 1} & \beta_m &= 4e^{\frac{-v}{18}} \\ \alpha_h &= 0.07e^{\frac{-v}{20}} & \beta_h &= \frac{1}{e^{\frac{30-v}{10}} + 1} \\ \alpha_n &= 0.01\frac{10 - v}{e^{\frac{10-v}{10}} - 1} & \beta_m &= 0.125e^{\frac{-v}{80}}. \end{aligned} \tag{2.1.5}$$

The variables m, n, and h describe the non-linear behaviours of the sodium activation, potassium activation, and sodium inactivation gates respectively. At the

C		Capacitance
g_l		Leak Conductance
g_K		Potassium Conductance
g_{Na}		Sodium Conductance
v_l		Leak Resting Potential
v_K		Potassium Resting Potential
v_{Na}		Sodium Resting Potential
i		Applied Current

Table 2.1: Definitions of Parameters used in the Hodgkin-Huxley Model.

time, these were chosen qualitatively to fit experimental data, but were subsequently shown to represent the gates within the channels. The sodium channel contains one h and three m gates while the potassium channel contains four n gates. All gates must be open for ions to pass through. The variables m, n, and h can be considered the probability that each gate is open, or the fraction of open channels. The product of these probabilities models the probability that a channel is open (or the fraction of open channels), assuming the gates are independent.

The parameters g_l, g_K, and g_{Na} are, respectively, the leak, potassium, and sodium conductances (a conductance is the reciprocal of a resistance). Essentially, the conductance is a measure of how easily a current can flow. Similarly, v_l, v_K, and v_{Na} are, respectively, the leak, potassium, and sodium resting potentials. The parameter i is an applied current.

The functions $\tau_n(v), \tau_m(v)$, and $\tau_h(v)$ describe the rate at which each of the m, n and h variables approach their steady states $n_\infty(v), m_\infty(v)$ and $h_\infty(v)$ respectively. Note that all of these are voltage dependent, characteristic of voltage gated ion channels [15] [16].

Each term in the $\frac{dv}{dt}$ equation represents a current. The leak current, given by $g_l(v_l - v)$ is the simplest. Alone, it would drive v toward v_l exponentially. The

Parameter	Value		Parameter	Value
g_l	.3		v_l	10.6
g_{Na}	120		v_{Na}	115
g_K	36		v_K	-12
C	1			

Table 2.2: Parameter values used by Hodgkin and Huxley (based on physiological values).

potassium current term, $g_K n^4(v_K - v)$ is similar, but it depends on the fourth power of n (one power for each gate). Clearly, this variable drives some non-linear approach to v_K. Similarly, the sodium current term $g_{Na} m^3 h(v_{Na} - v)$ drives some non-linear approach to v_{Na}. Since $v_{Na} \gg v_l > v_K$, the sodium current tends to increase v while the other current terms tend to decrease v. The different nonlinearities of each of these terms, and their different time scales gives rise to the oscillatory dynamics. The applied current term, i, can model an external stimulus and its rôle will be discussed in more detail in Chapter 3.

The behaviour of this system varies dramatically depending on the parameters and initial conditions. There can be an asymptotically stable fixed point or a train of action potentials. A good qualitative analysis of this system can be found in [16], but here solutions to the Hodgkin-Huxley equations will be generated numerically. Figure 2.2, created using the software package XPP, shows examples for parameters given in Table 2.2. More importantly, Figure 2.3, motivated by the analysis in [16], shows a phase portrait of a single action potential in the $v - n$ cross section of $\mathbb{R}^4$, including the nullclines when $m = m_\infty(v)$, $h = 0.8 - n$ (consistent with the analysis of [16]) where parameters are as in Figure 2.2. It is the general shapes of the nullclines that gives rise to the oscillations and permit simplification. Note that the v-nullcline is roughly cubic and the n-nullcline is roughly sigmoid.

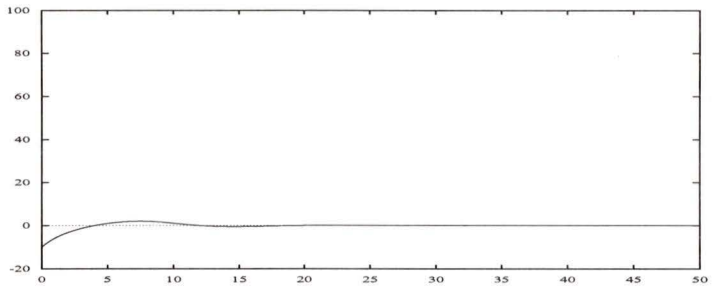

(a)

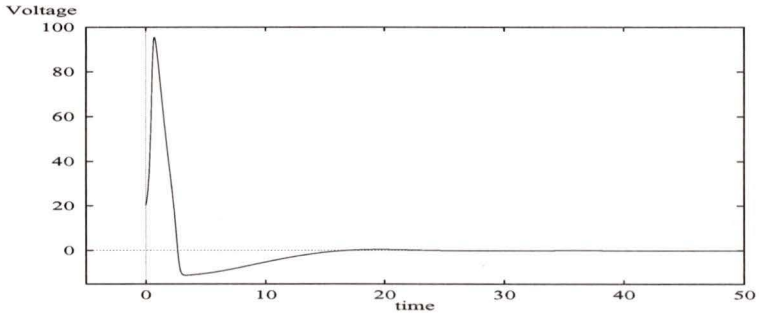

(b)

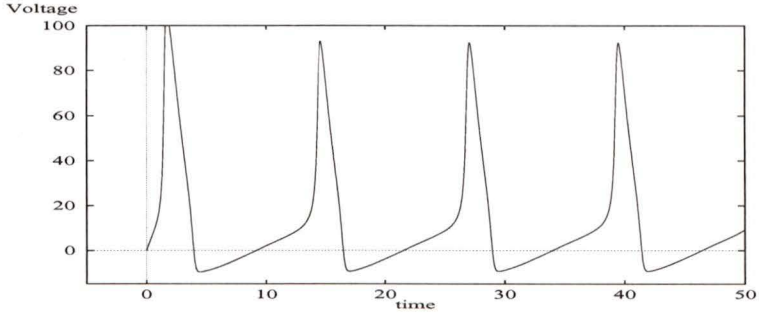

(c)

Figure 2.2: Some numerical solutions to the Hodgkin-Huxley equations. Parameters are as given in Table 2.2, the parameter i has values 0 in (a) and (b) and 8 in (c). Note that (a) and (b) differ only by initial conditions

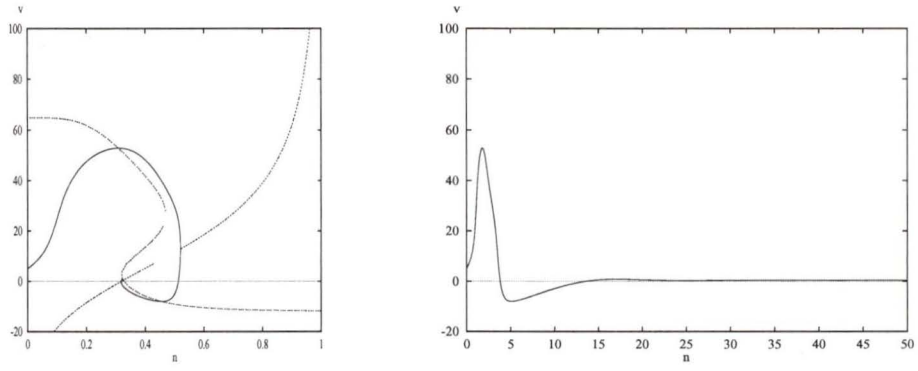

(a) Phase Portrait in v and n including nullclines

(b) $v(t)$ Computed Numerically

Figure 2.3: Phase portrait (a) and numerical solution (b) of the reduced Hodgkin-Huxley equations. The variable m is held in its steady state, and h is taken as $0.8-n$, so the resulting system is two-dimensional. Parameters are as in Table 2.2 with $i = 8$.

2.1.2 Morris-Lecar Equations

In the spirit of the Hodgkin-Huxley equations, Morris and Lecar [20] sought to describe the dynamics of the barnacle muscle fibre. In this cell, dynamics are slower, and there are no action potentials, but appropriate parameter values give oscillatory solutions. However, the form of the model, and the underlying reasoning, based on Kirchoff's laws are similar. This model has the advantage of being of lower dimension than that of Hodgkin and Huxley. Here, the principal ion species are calcium and potassium. The full Morris-Lecar system is

$$\begin{aligned} C\frac{dv}{dt} &= g_l(v_l - v) + g_K n(v_K - v) + g_{Ca} m(v_{Ca} - v) + i_{app} \\ \frac{dn}{dt} &= \lambda_n(v)(n_\infty(v) - n) \\ \frac{dm}{dt} &= \lambda_m(v)(m_\infty(v) - m) \end{aligned} \tag{2.1.6}$$

C		Capacitance
g_l		Leak conductance
g_K		Potassium conductance
g_{Ca}		Calcium conductance
v_l		Leak resting potential
v_K		Potassium resting potential
v_{Ca}		Calcium resting potential
v_a		Potential at which $m_\infty(v) = 0.5$
v_b		Reciprocal of slope of voltage dependence of $m_\infty(v)$
v_c		Potential at which $n_\infty(v) = 0.5$
v_d		Reciprocal of slope of voltage dependence of $n_\infty(v)$
φ_m		Rate constant for calcium channel opening
φ_n		Rate constant for potassium channel opening
i		Applied current

Table 2.3: Definitions of parameters used in the Morris-Lecar equations

where the functions

$$\begin{aligned} n_\infty(v) &= \frac{1}{2}\left(1 + \tanh\left(\frac{v - v_c}{v_d}\right)\right) \\ \lambda_n(v) &= \varphi_n \cosh\left(\frac{v - v_c}{2v_d}\right) \\ m_\infty(v) &= \frac{1}{2}\left(1 + \tanh\left(\frac{v - v_a}{v_b}\right)\right) \\ \lambda_m(v) &= \varphi_m \cosh\left(\frac{v - v_a}{2v_b}\right) \end{aligned}$$

are chosen qualitatively and parameters are as defined in Table 2.3. The functions $m_\infty(v), n_\infty(v), \lambda_m(v)$ and $\lambda_n(v)$ describe, respectively, the steady state m value, the steady state n value, the relaxation rate of the calcium channels and the relaxation rate of the potassium channels.

Here, the nonlinear dependence of the channels on the potential difference is described qualitatively by the sigmoidal functions $m_\infty(v)$ and $n_\infty(v)$. Under the assumption that the dynamics of m are very fast, m is considered to be instantaneously

in its steady state, so the system can be reduced to

$$\begin{aligned} C\frac{dv}{dt} &= g_l(v_l - v) + g_K n(v_K - v) + g_{Ca} m_\infty(v)(v_{Ca} - v) + i_{app} \qquad (2.1.7) \\ \frac{dn}{dt} &= \lambda_n(v)(n_\infty(v) - n). \end{aligned}$$

The variables are v, which represents the voltage drop across a cell membrane, and n, which represents the fraction of open potassium ion channels.

Similar to the Hodgkin-Huxley equations, the parameters g_l, g_K, and g_{Ca} are, respectively, the leak, potassium, and calcium conductances. The parameters v_l, v_K, and v_{Ca} are, respectively, the leak, potassium, and calcium resting potentials, and i is an applied current. The parameters φ_m and φ_n attenuate the relaxation times of the channel variables.

Each term in the $\frac{dv}{dt}$ equation represents a current, but the opposing ions are calcium and potassium instead of sodium and potassium as in the Hodgkin-Huxley model. The leak current drives v toward v_l exponentially. The potassium current drives v toward v_K and the calcium current drives v toward v_{Ca}, though there is no dynamic variable left to describe the behaviour of the calcium channels. Here, due to their respective signs, the calcium current term opposes the other two, and the calcium and potassium non-linearities give rise to oscillations for appropriate choices of the parameters.

The $\frac{dn}{dt}$ equation contains only one term driving some non-linear approach to $n_\infty(v)$. The factor $\lambda_n(v)$ determines the rate of this approach. The functions $n_\infty(v)$ and $\lambda_n(v)$ are chosen to fit the data from voltage clamp experiments as stated in [20].

The behaviour of this 2-D system can be inferred from its phase plane. Figure 2.4 shows the vector field and the intersection of nullclines for parameters as given in Table 2.4. Adjusting the parameter i effectively shifts the v-nullcline horizontally.

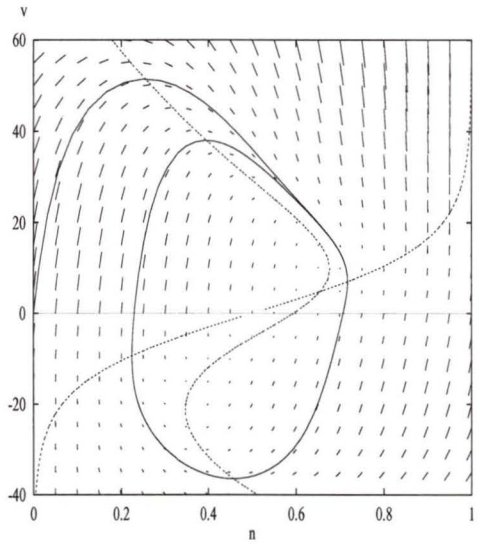

Figure 2.4: Phase portrait including nullclines (dotted) and solution trajectory for a single Morris-Lecar neuron. Parameters are as in Table 2.4 except i=0.4. The n-nullcline is sigmoid and the v-nullcline is cuboid

Parameter	Value		Parameter	Value
g_l	.005		v_l	-50
g_{Ca}	.015		v_{Ca}	100
g_K	.02		v_K	-80
v_a	0		v_b	15
v_c	0		v_d	15
φ_n	.002			

Table 2.4: A sample of the physiologically reasonable parameter values used by Skinner et al [31] for a Morris-Lecar neuron.

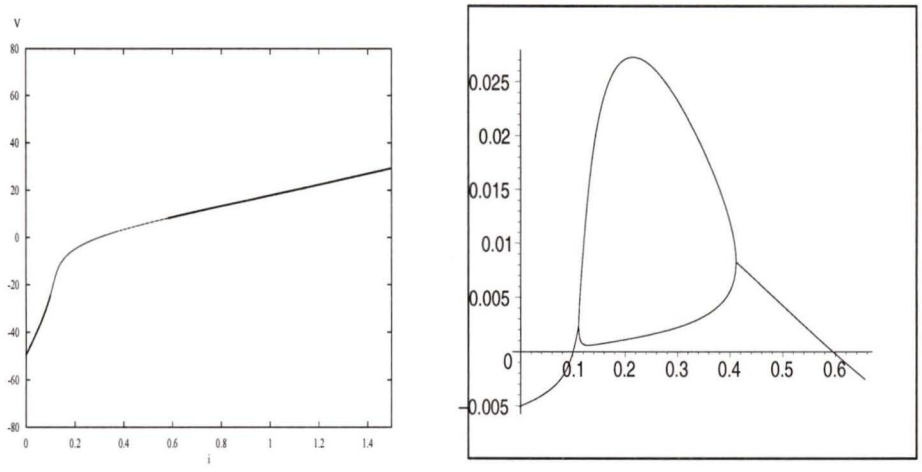

(a) Bifurcation diagram

(b) Real parts of eigenvalues vs. i

Figure 2.5: Bifurcation diagram (a) and eigenvalue plot (b) illustrating the change in stability of the unique fixed point. The heavy line in (a) denotes stability. In (b) two curves exist when the eigenvalues are real.

Setting $\frac{dv}{dt} = \frac{dn}{dt} = 0$ in (2.1.7) gives the equations of the nullclines:

$$\begin{aligned} v &= \frac{g_l v_l + g_K n v_K + g_{Ca} m_\infty(v) v_{Ca} + i}{g_l + g_K n + g_{Ca} m_\infty(v)} \\ n &= n_\infty(v) \end{aligned}$$

so the unique fixed point is easily identified, at least numerically.

Setting $\frac{dv}{dt} = 0$ in (2.1.7) and rearranging gives i as a function of v and n. Of course the linearization matrix has entries that are functions of v and n also. Since at fixed points $n = n_\infty$ all entries in the linearization matrix can be written as functions of v alone, so the corresponding eigenvalues can be computed as functions of v, and a parametric plot gives the equilibrium voltage as a function of the applied current. Figure 2.5(a) shows a bifurcation diagram computed numerically using the software package AUTO. Note that as i increases, the equilibrium voltage also increases, but

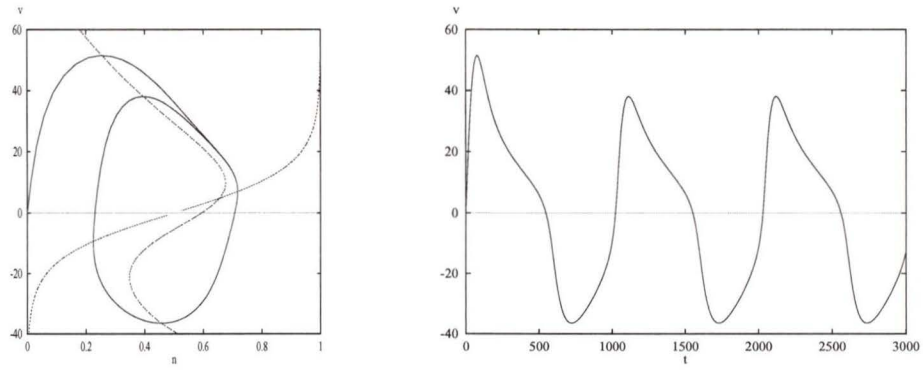

(a) Phase Portrait

(b) $v(t)$ computed numerically

Figure 2.6: Phase portrait (a) and numerical solution (b) to the Morris-Lecar equations (2.1.7). Parameters are given in Table 2.4 and $i = 0.4$.

changes stability. Figure 2.5(b) shows a plot of the real parts of the eigenvalues as functions of the parameter i.

Since solutions are bounded, and there is only one fixed point, application of the Poincaré-Bendixson theorem shows that if the real parts of the eigenvalues are positive, there exists a stable periodic orbit (shown in Figure 2.6). As the parameter i increases from about 0.1, Hopf bifurcation (supercritical) gives rise to limit cycles. Further increasing i past about 0.6 results in another Hopf bifurcation, causing limit cycles to cease. See the paper by Morris and Lecar [20] for a more complete analysis.

2.1.3 FitzHugh-Nagumo Equations

A polynomial simplification of the Hodgkin-Huxley equations was presented by FitzHugh and Nagumo in 1964 [16]. Here the nullclines (compare Figure 2.7(a) to Figure 2.3(a)) in the 2D vector field of the fast-slow subsystem of the Hodgkin-Huxley equations are approximated by cubic and linear polynomials. So the Hodgkin-Huxley

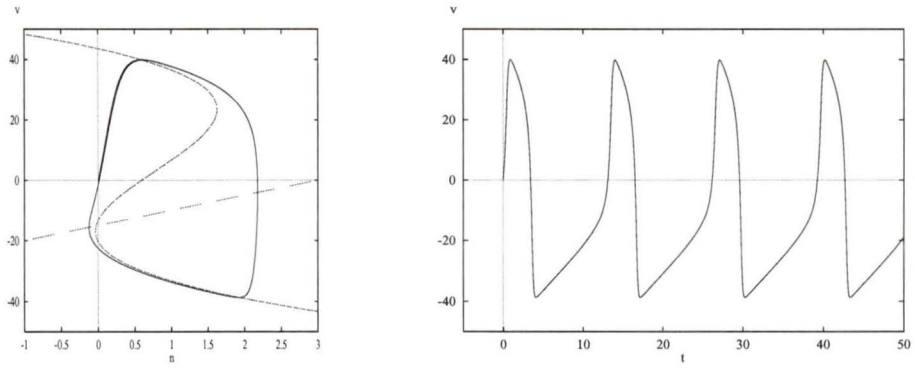

(a) Phase Portrait

(b) $v(t)$ computed numerically

Figure 2.7: Phase portrait (a) and numerical solution (b) of the FitzHugh-Nagumo equations. Parameters are $i = 0.6$ and $\varepsilon = 0.02$

system is approximated by:

$$\begin{aligned} \varepsilon \frac{dv}{dt} &= 5 \times 10^5 v(v+30)(40-v) - n + i \\ \frac{dn}{dt} &= \frac{1}{60}(v - 5n + 15). \end{aligned} \tag{2.1.8}$$

This is a relaxation oscillator whose behaviour is determined almost completely by the intersections of the nullclines. As in the previous two models, there can be a stable fixed point or an unstable fixed point about which the solutions oscillate. If ε is small, the dynamics of v are much faster than those of n, giving rise to the spikes. For appropriate choices of the parameters, the nullclines intersect exactly once in a way that permits oscillations much like the Hodgkin-Huxley action potentials. Comparison between a train of Hodgkin-Huxley action potentials and a train of FitzHugh-Nagumo action potentials suggests that the FitzHugh-Nagumo model is at least a qualitatively reasonable 2D description of the Hodgkin-Huxley model describing spiking neurons. See [16] for a thorough analysis of the FitzHugh-Nagumo equations.

2.2 Equations Describing Connections Between Neurons

A variety of models exist, ranging in complexity, to describe synapses or other connections between cells. Of course it is imperative that these models describe how one (presynaptic) cell affects another (postsynaptic) cell. As before, there is a tradeoff between modelling this connection physiologically well and describing it simply. Perhaps the most obvious approach to coupling two neurons is simply to add a synaptic current term of the form $g_{syn}s(v - v_{syn})$ to the $\frac{dv}{dt}$ equation of the cellular models already described.

The variable s is analogous to the channel variables in the other terms. If it ranges from 0 to 1, then the product $g_{syn}s$ represents the synaptic conductance, so the synaptic current term drives some nonlinear approach to v_{syn}, the synaptic resting potential. It is well known [15] that for many synapses, s depends at least on the presynaptic potential, so such a term can be used to couple neurons. For example, adding a synaptic term to a Morris-Lecar system, a Morris-lecar neuron can be coupled to a FitzHugh-Nagumo neuron as follows:

$$\begin{aligned}
\frac{dv_1}{dt} &= g_l(v_l - v_1) + g_K n_1(v_K - v_1) + g_{Ca} m_\infty(v_1)(v_{Ca} - v_1) + g_{syn}s(v_{syn} - v_1) + i \\
\frac{dn_1}{dt} &= \lambda(v_1)(m_\infty(v_1) - n_1) \\
\varepsilon\frac{dv_2}{dt} &= 5 \times 10^5 v_2(v_2 + 30)(40 - v_2) - n_2 + i \qquad (2.2.1) \\
\frac{dn_2}{dt} &= \frac{1}{60}(v_2 - 5n_2 + 15) \\
\tau\frac{ds}{dt} &= \frac{s_\infty - s}{1 - s_\infty}.
\end{aligned}$$

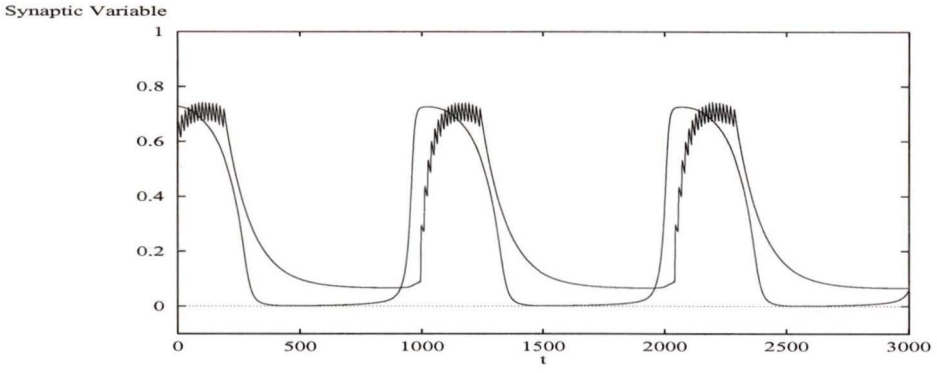

Figure 2.8: A comparison of s (rough), from (2.2.1), and the sigmoidal approximation $S(v_1)$ (smooth), computed numerically.

where

$$s_\infty = \tanh \frac{v_2 - v_a}{v_b} \tag{2.2.2}$$

The parameter g_{syn} is a synaptic conductance, and v_{syn} is a synaptic resting potential. The parameters v_a and v_b determine the shape of the sigmoid, and all other functions and parameters are as described in Section 2.1.2. In the extra current term, the variable s accounts for the nonlinear dependence on the synapse and acts like the variables describing the nonlinearities for each of the other current terms.

Of course there are many levels of complexity involved in describing synapses, and, indeed, many different kinds of synapses, so this serves only as an example.

A much simpler approach is to ignore the dynamics of the synapse and use a qualitatively similar function to approximate the synaptic variable. The important part of the connection, the post synaptic potential, can be accounted for qualitatively by a nonlinear function of the presynaptic voltage. Figure 2.8 shows how the sigmoid function $S(v_{pre}) = \frac{1}{2}\left[1 + \tanh \frac{v_{pre}}{15}\right]$ approximates the synaptic variable $s(v_{pre})$ in (2.2.1), where v_{pre} refers to the presynaptic voltage. Both $S(v)$ and $s(v)$ are computed

numerically.

Regardless of the particular form of the synaptic variable, it can be used to provide an additional current term of the form $g_{syn}S(v_{pre})(v-v_{syn})$ or $g_{syn}s_i(v-v_{syn})$ to the $\frac{dv}{dt}$ equation of any of the FitzHugh-Nagumo, Morris-Lecar, or Hodgkin-Huxley systems. In any case, the term describes the link between the presynaptic and postsynaptic cells, thereby coupling them.

2.3 Equations on $\mathbb{T}^n$

A far simpler coarse-scale approach is to neglect specific dynamics within each CPG and consider it an arbitrary oscillator with, of course, an intrinsic limit cycle. All of the important information describing the behaviour of the large system can be described clearly by the phase of each oscillator, or, more to the point, the phase *differences* between coupled oscillators [1] [2] [14].

An equation describing the phase of a single oscillator with intrinsic frequency ω is:

$$\frac{d\theta}{dt} = \omega. \tag{2.3.1}$$

Coupled together, n such oscillators are described by equations of the form

$$\frac{d\theta_i}{dt} = \omega_i + \sum_{j=1}^{n} H_{ij}(\theta_j - \theta_i) \tag{2.3.2}$$

where $\theta_j - \theta_i$ defines the phase difference between the i^{th} and j^{th} oscillators and the functions H_{ij} describe the effect that the j^{th} oscillator has on the i^{th} ($H_{ii}(0) = 0$) [14]. For example, oscillators arranged as in Figure 2.9 are described by equations of the

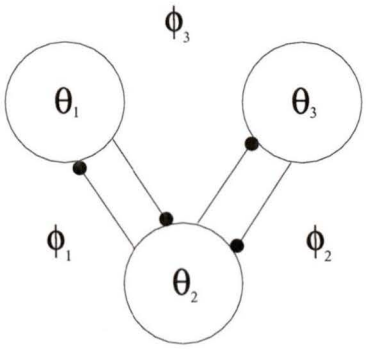

Figure 2.9: Three identical oscillators arranged in a chain.

form

$$\begin{aligned} \frac{d\theta_1}{dt} &= \omega_1 + H_{12}(\theta_2 - \theta_1) \\ \frac{d\theta_2}{dt} &= \omega_2 + H_{21}(\theta_1 - \theta_2) + H_{23}(\theta_3 - \theta_2) \\ \frac{d\theta_3}{dt} &= \omega_3 + H_{32}(\theta_2 - \theta_3) \end{aligned} \tag{2.3.3}$$

To study the phase *differences* between these oscillators, let

$$\phi_i = \theta_{i+1} - \theta_i \tag{2.3.4}$$

where $\theta_{i+3} = \theta_i$. So for the arrangement in Figure 2.9

$$\begin{aligned} \frac{d\phi_1}{dt} &= \omega_2 - \omega_1 + H_{23}(\phi_2) + H_{21}(-\phi_1) - H_{12}(\phi_1) \\ \frac{d\phi_2}{dt} &= \omega_3 - \omega_2 + H_{32}(-\phi_2) - H_{23}(\phi_2) - H_{21}(-\phi_1) \\ \frac{d\phi_3}{dt} &= \omega_1 - \omega_3 + H_{12}(\phi_1) - H_{32}(-\phi_2) \end{aligned} \tag{2.3.5}$$

The form of the functions H_{ij} determining how the phases interact can be derived from the cellular equations [1] [2] [14], and will be discussed in more detail starting in Chapter 4. The important information here is that the rate of change of phase of an oscillator with a stable limit cycle is its natural rate of change plus that induced by the other oscillators.

2.4 Selection of Appropriate Equations

The ganglia of *Emerita* likely contain many non-spiking and spiking neurons [5]. In order to transmit signals over distances, spiking neurons are required [15], so models describing both must be incorporated. Neurons within each CPG will be described by Morris-Lecar equations, and neurons connecting CPGs will be described by either by Hodgkin-Huxley, or by FitzHugh-Nagumo equations, depending on the appropriate level of simplicity.

In Chapter 3, each CPG will be considered as a single Morris-Lecar neuron. Connections between these will be represented by the sigmoid functions in order to keep the dimension of the system low. In Chapter 4, the equations used in Chapter 3 will be reduced to phase equations on $\mathbb{T}^3$. In Chapter 5, the CPGs will be elaborated to include three Morris-Lecar neurons each, along with synaptic variables and FitzHugh-Nagumo neurons between CPGs. These will be solved numerically for comparison to one another, and then reduced, as in Chapter 4, to equations on $\mathbb{T}^3$ for further analysis.

Chapter 3

Coupled $2D$ Oscillator Model

To begin analyzing a system of coupled CPGs, it is illustrative first to consider an over-simplified case in which each is described by equations governing the dynamics of a single neuron. Even in this simple arrangement, analysis is difficult, but the existence of limit cycles in special cases can be shown analytically, and supported numerically.

Consider the two arrangements of neural oscillators depicted in Figure 3.1 where V_1 refers to the left fourth leg, V_3 refers to the right fourth leg, and V_2 refers to the pair of uropods. The first (Figure 3.1(a)) represents a network of CPGs in which there is no direct bilateral connection between neurons driving each leg. The second (Figure 3.1(b)) represents a network in which bilateral connections between the legs exist and are of the same nature as those coupling the legs to the uropods.

This chapter addresses the existence and stability of limit cycles in these networks if the reduced Morris-Lecar equations are used to describe each CPG. Numerical solutions suggest that when the coupling between left and right legs is zero, there exists a stable limit cycle where the left and right legs beat in phase with one another, with both about half a cycle out of phase with the uropods. Also, numerical solutions

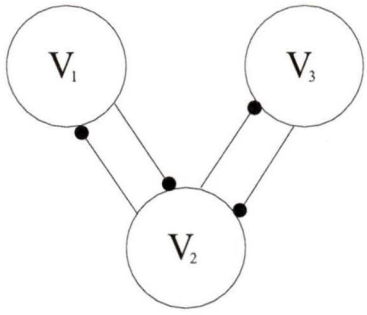

(a) No direct bilateral coupling ($\mathbb{Z}_2$ symmetry

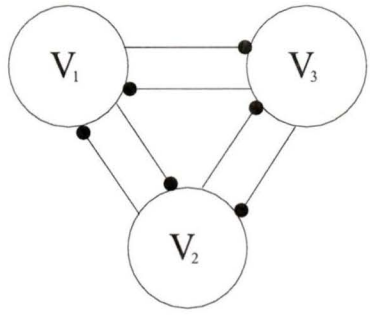

(b) Coupling identical between all oscillators ($\mathbb{D}_3$ symmetry)

Figure 3.1: Two symmetric arrangements of CPGs.

suggest that if coupling between all oscillators is of equal strength and type, there exists a stable limit cycle in which all appendages beat $\frac{1}{3}$ of a cycle out of phase with each of the others. Finally, numerical solutions suggest that if coupling strengths between oscillators 1 and 3 are varied, intermediate phase differences are possible. This chapter discusses the existence and stability of limit cycles in the two symmetric cases. Due to the complexity of the system, asymmetric cases will be treated in later chapters after the equations have been simplified.

3.1 No Bilateral Connections ($\mathbb{Z}_2$ symmetry)

In the absence of direct bilateral connections between the left and right legs, the oscillators are effectively arranged in a chain as shown in 3.1(a). Using a Morris-Lecar system of equations (as described in Section 2.1.2) to describe each oscillator, and coupling them using simple sigmoid functions of the presynaptic voltages, equations

Parameter	Value		Parameter	Value
g_l	.005		v_l	-50
g_{Ca}	.015		v_{Ca}	100
g_K	.02		v_K	-80
g_{syn}	.0025		v_{syn}	-80
φ	.002			

Table 3.1: Parameter values including coupling parameters

describing the network are:

$$\frac{dV_i}{dt} = F(V_i) + g_{syn}G_i(V_1, V_2, V_3) \tag{3.1.1}$$

with

$$F(V_i) = \begin{bmatrix} g_l(v_l - v_i) + g_K n_i(v_K - v_i) + g_{Ca}m_\infty(v_i)(v_{Ca} - v_i) + i_{app} \\ \lambda_n(v_i)(n_\infty(v_i) - n_i) \end{bmatrix}$$

$$G_1(V_1, V_2, V_3) = \begin{bmatrix} S(v_2)(v_{syn} - v_1) \\ 0 \end{bmatrix}$$

$$G_2(V_1, V_2, V_3) = \begin{bmatrix} (S(v_1) + S(v_3))(v_{syn} - v_2) \\ 0 \end{bmatrix}$$

$$G_3(V_1, V_2, V_3) = \begin{bmatrix} S(v_2)(v_{syn} - v_3) \\ 0 \end{bmatrix}$$

where $V_i = \begin{bmatrix} v_i \\ n_i \end{bmatrix} \in \mathbb{R}^2$, $i \in \{1, 2, 3\}$, $\lambda_n(x)$ is as described in Section 2.1.2, i_{app} takes the place of i from previous sections, and $S(v) = \frac{1}{2}\left[1 + \tanh\frac{v}{15}\right]$. Clearly, there is bilateral ($\mathbb{Z}_2$) symmetry in these equations and in the physical structure of the network, so a solution with the same symmetry is expected [8] [10]. Indeed, using physiologically reasonable [29] parameters given in Table 3.1 there exists a stable limit cycle in which oscillators 1 and 3 follow identical trajectories and are together

approximately half a cycle out of phase with oscillator 2. Of course this is a qualitative assertion since V_2 follows a different trajectory than V_1 and V_3. In Figure 3.2, each of the v_i variables are graphed together over several oscillations starting with "random" initial conditions. The figure illustrates the system's tendency toward a bilaterally symmetric limit cycle. Over very few cycles the V_1 and V_3 variables align and thenceforth remain together.

The existence of a limit cycle in this system relies mainly on the fact that, uncoupled, each oscillator tends to its own limit cycle. First consider $g_{syn} = 0$, making $G_i = 0$. Clearly the oscillators are uncoupled and each tends to its own limit cycle so the 6D system has a pseudo-stable limit cycle (the direct sum of the three). Of course, in this case the limit cycle phase relationship between the oscillators is very sensitive to initial conditions, so the system is not robust. Allowing g_{syn} to be small and positive imposes relationships between the variables.

For g_{syn} small, the coupling terms can be considered perturbations to each of the oscillators. If each has a stable limit cycle (call it γ_i) and is not close to a bifurcation point, it is known that the stable manifold (limit cycle) will persist after small perturbation [6] [27]. Therefore, solution trajectories of the full system should be near the manifold $\gamma_1 \times \gamma_2 \times \gamma_3$.

Inspection of equations (3.1.1) shows that if V_1 and V_3 are ever equal, then they will be equal forever, since $\frac{dV_1}{dt} = \frac{dV_3}{dt}$. Similar inspection reveals that if $V_1 = V_2 = V_3$, then V_2 separates from the others since $\frac{dV_2}{dt} \neq \frac{dV_1}{dt}$ (or $\frac{dV_3}{dt}$). Numerical solution (Figure 3.3) shows that if V_1 and V_3 are close, then their values approach each other.

So with no direct coupling between the oscillators driving the right and left legs, the system of three Morris-Lecar CPGs with reciprocal inhibition between legs and

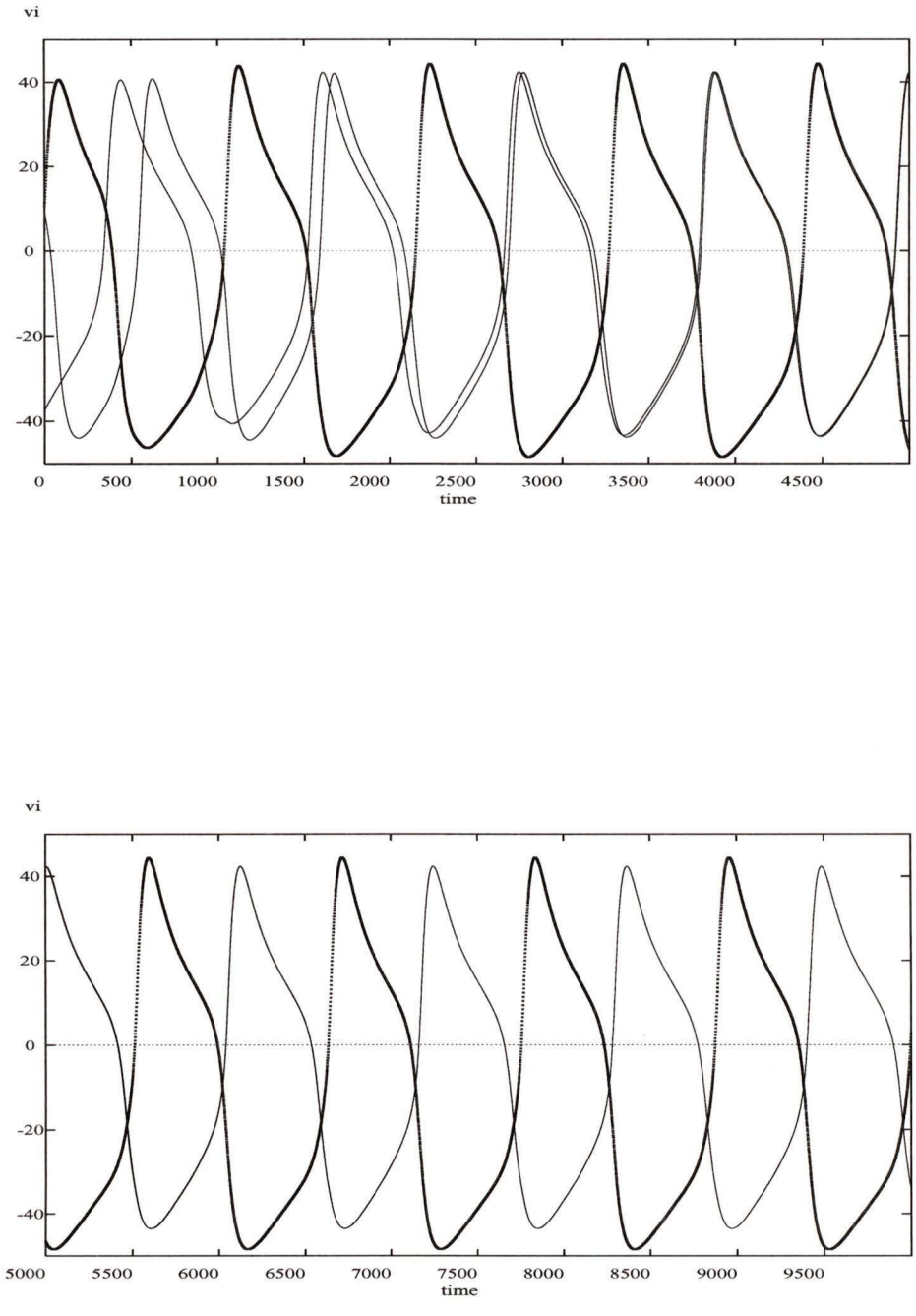

Figure 3.2: Limit cycles of the v variable of each oscillator computed numerically. The dashed (heavy) curve is v_2 and the light curves are v_1 and v_3.

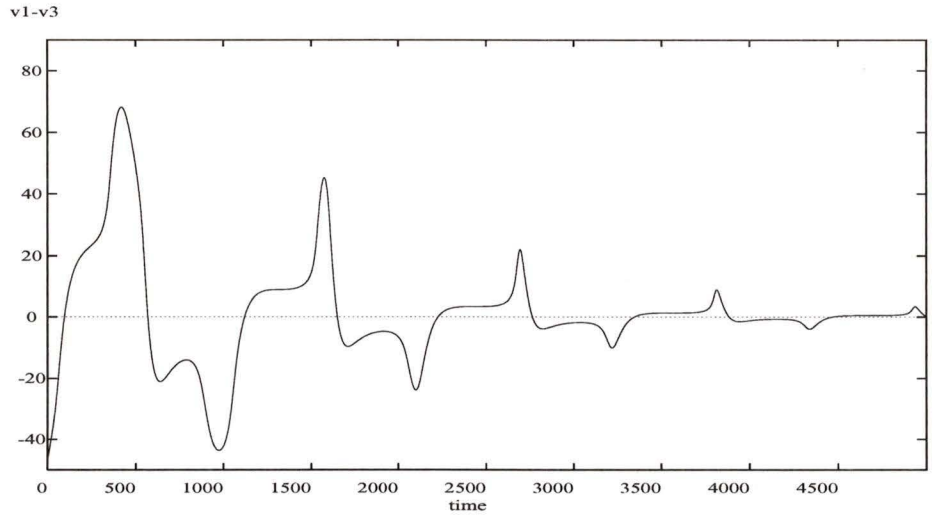

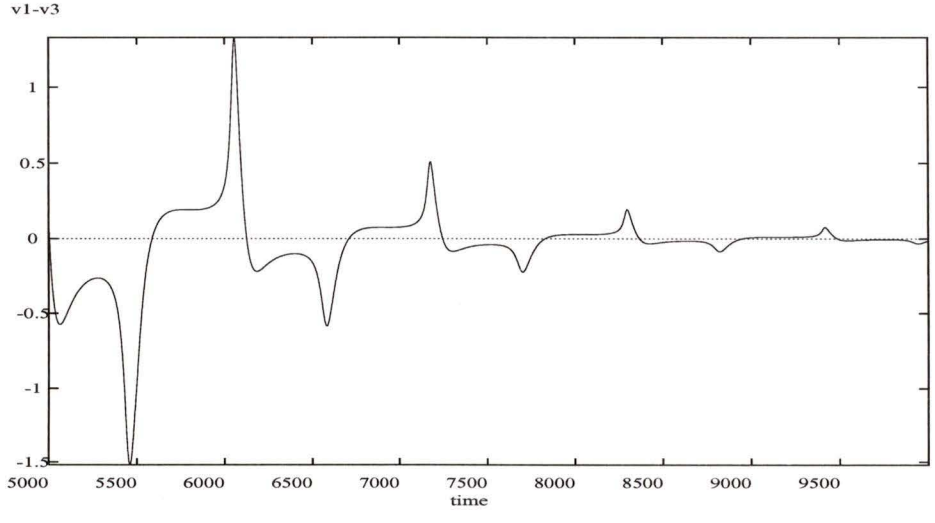

Figure 3.3: Numerical solution of the *difference* between v_1 and v_3 as the trajectories align. The curves appear similar, but the voltage scale is adjusted in the second to illustrate detail.

uropods tends to a limit cycle in which all appendages cycle in a manner indicative of the early stages of a dig.

3.2 Fully Symmetric Connection Patterns ($\mathbb{D}_3$ symmetry)

Consider now a similar system to that in Section 3.1, but with bilateral connections between CPGs. Describing this special symmetry case using Morris-Lecar equations, the system of reciprocally inhibitory oscillators with all synaptic connections of equal weight, as shown in Figure 3.1(b), is given by equations of the form

$$\frac{dV_i}{dt} = F(V_i) + g_{syn}G_i(V_1, V_2, V_3) \tag{3.2.1}$$

$$F(V_i) = \begin{bmatrix} g_l(v_l - v_i) + g_K n_i(v_k - v_i) + g_{Ca}m_\infty(v_i)(v_{Ca} - v_i) + i_{app} \\ \lambda(v_i)(n_\infty(v_i) - n_i) \end{bmatrix} = \begin{bmatrix} p_i \\ q_i \end{bmatrix}$$

$$G_i(V_1, V_2, V_3) = \begin{bmatrix} (S(v_{i+1}) + S(v_{i+2}))(v_{syn} - v_i) \\ 0 \end{bmatrix}$$

where $V_i = \begin{bmatrix} v_i \\ n_i \end{bmatrix} \in \mathbb{R}^2$, $i \in \{1, 2, 3\}$, $v_{i+3} = v_i$, $n_{i+3} = n_i$, and $\lambda_n(x)$ and $S(x)$ are as before. These equations belong to the symmetry group $\mathbb{D}_3$ indicating that there should be solutions V_i with the same symmetries [8] [9]. Numerical computation with parameters as given in Table 3.1 yields such solutions shown in Figure 3.4 and motivates the search for a proof of their existence. Finding fixed points as they depend on the parameter i_{app} and determining stability of the system nearby is the first step. It is easy to write i_{app} as a function of v_{eq}, so showing that $i_{app}(v_{eq})$ has an inverse

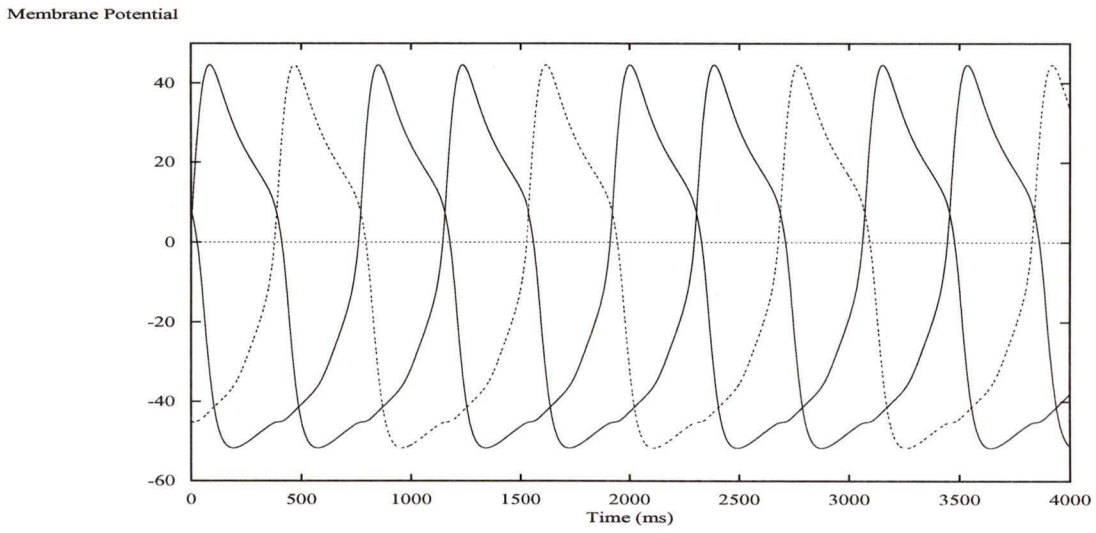

Figure 3.4: Limit cycles of the v variable of each oscillator (equations (3.2.1)) computed numerically. The dashed curve is v_2 and the solid curves are v_1 and v_3.

is sufficient to prove that v_{eq} is a function of i_{app}. After obtaining v_{eq}, n_{eq} can be computed, and stability can be found using linearization.

By symmetry, assume that the system (3.2.1) has a fixed point where $n_1 = n_2 = n_3 = n_{eq}$ and $v_1 = v_2 = v_3 = v_{eq}$. Clearly, in order to have $\frac{dn_i}{dt} = 0, n_{eq} = n_\infty(v_{eq})$. So setting $\frac{dv_i}{dt} = 0$, and substituting for n_{eq} to find v_{eq}:

$$0 = g_l(v_l - v_{eq}) + g_K n_{eq}(v_K - v_{eq}) + g_{Ca} m_\infty(v_{eq})(v_{Ca} - v_{eq}) + g_{syn}(2S(v_{eq}))(v_{syn} - v_{eq}) + i_{app} \tag{3.2.2}$$

With parameters given in Table 2.3, $n_{eq} = m_\infty(v_{eq}) = S(v_{eq})$, so the expression

$$i_{app} = g_l(v_{eq} - v_l) + S(v_{eq})[g_K(v_{eq} - v_K) + g_{Ca}(v_{eq} - v_{Ca}) + 2g_{syn}(v_{eq} - v_{syn})] \tag{3.2.3}$$

at least implicitly defines this equilibrium voltage as a function of the parameter, i_{app} (see Figure 3.5), representing an applied current, which will be used as a bifurcation parameter. With the other parameters as given in Table 3.1, the derivative of $i_{app}(v_{eq})$ satisfies

$$\frac{di_{app}}{dv_{eq}} = 0.025 + \frac{1}{30}\left(1 - \tanh^2\left(\frac{v_{eq}}{15}\right)\right)(0.04v_{eq} + 0.5) + 0.02\tanh\left(\frac{v_{eq}}{15}\right).$$

Further, since $\frac{di_{app}}{dv_{eq}} > 0.02$ for at least one v_{eq} ($v_{eq} = 6$ for example), if $\frac{di_{app}}{dv_{eq}} = 0$ for any value of v_{eq} then there exists some other v_{eq} such that

$$0 = 0.025 + \frac{1}{30}\left(1 - \tanh^2\left(\frac{v_{eq}}{15}\right)\right)(0.04v_{eq} + 0.5)$$

so

$$\frac{-0.75}{1 - \tanh^2\left(\frac{v_{eq}}{15}\right)} = 0.04v_{eq} + 0.5$$

which simplifies to

$$-0.75\cosh^2\left(\frac{v_{eq}}{15}\right) = 0.04v_{eq} + 0.5.$$

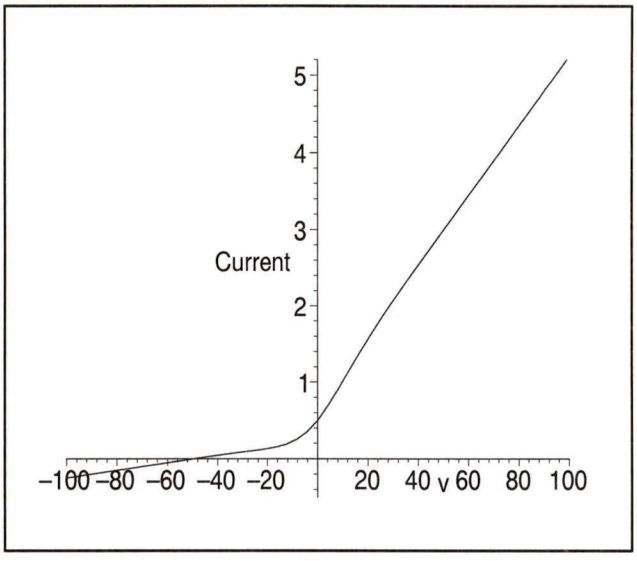

Figure 3.5: Graph of the function $i_{app}(v_{eq})$, equation (3.2.3)

It is clear that graphs of the left hand side and the right hand side never intersect, so $\frac{di_{app}}{dv_{eq}} \neq 0$ for any v_{eq}. Since $i_{app}(v_{eq})$ is monotonic increasing function of v_{eq} (see Figure 3.5), it has an inverse $v_{eq}(i_{app})$, so there is exactly one equilibrium voltage for any value of i_{app}.

Linearization (recall Section 2.1.2) shows that each of the uncoupled oscillators undergo Hopf bifurcations when $i_{app} \cong 0.1$ and $i_{app} \cong 0.59$. A similar procedure, discussed below, identifies values of i_{app} for which this 6D system undergoes Hopf-type bifurcations.

3.2.1 Linearizing the system near the fixed points

With the fixed point values identified, the linearization matrix can be evaluated and aspects of the behaviour of the system can be inferred. Let $X = V_1 \bigoplus V_2 \bigoplus V_3 \in \mathbb{R}^6$.

Near the fixed point X_0, the system of equations (3.2.1) behaves like the system

$$\frac{dX}{dt} = M(X - X_0) \tag{3.2.4}$$

where M is the Jacobian matrix of the vector field of (3.2.1) evaluated at the fixed point determined by i_{app}. Exploiting the symmetries in the partial derivatives,

$$M = \begin{bmatrix} A & B & B \\ B & A & B \\ B & B & A \end{bmatrix}$$

where

$$A = \begin{bmatrix} \frac{\partial p_1}{\partial v_1} & \frac{\partial p_1}{\partial n_1} \\ \frac{\partial q_1}{\partial v_1} & \frac{\partial q_1}{\partial n_1} \end{bmatrix}_{X_0}$$

$$B = \begin{bmatrix} \frac{\partial p_1}{\partial v_2} & 0 \\ 0 & 0 \end{bmatrix}_{X_0}$$

The matrix A describes the intrinsic properties of each oscillator, and B describes connections between oscillators, depending on g_{syn}. According to work by Golubitsky and others [9] [10], the eigenvalues of M are those of $A+2B$ and those of $A-B$ with multiplicity 2, which can be calculated easily. Let

$$A^* = A + 2B = \begin{bmatrix} \frac{\partial p_1}{\partial v_1} + 2\frac{\partial p_1}{\partial v_2} & \frac{\partial p_1}{\partial n_1} \\ \frac{\partial q_1}{\partial v_1} & \frac{\partial q_1}{\partial n_1} \end{bmatrix}_{X_0}$$

and

$$B^* = A - B = \begin{bmatrix} \frac{\partial p_1}{\partial v_1} - \frac{\partial p_1}{\partial v_2} & \frac{\partial p_1}{\partial n_1} \\ \frac{\partial q_1}{\partial v_1} & \frac{\partial q_1}{\partial n_1} \end{bmatrix}_{X_0}$$

Note that A^* and B^* differ only in their $(1,1)$ entries. The matrix A^* has eigenvalues $\lambda(A^*)$ satisfying $\lambda^2 - (\mathrm{tr}A^*)\lambda + \det A^* = 0$ and B^* has eigenvalues $\lambda(B^*)$

satisfying $\lambda^2 - (\mathrm{tr}B^*)\lambda + \det B^* = 0$. The quadratic formula gives these eigenvalues as functions of the equilibrium value v_{eq}, so a parametric plot reveals the real parts of the eigenvalues as functions of the bifurcation parameter i_{app}, as shown in Figure 3.6.

Clearly, if the parameter g_{syn} were zero, $B = 0$, and the eigenvalues would be those of the uncoupled system with multiplicity three. As i_{app} increases from zero, with $g_{syn} = 0.0025$ first the real parts of the eigenvalues from B^* change sign when $i_{app} \approx 0.102$, giving rise to a degenerate Hopf bifurcation. As i_{app} is increased further, those of A^* change sign so that all eigenvalues are complex with positive real parts. When $i_{app} \approx .66$ the real part of the eigenvalues corresponding to A^* go negative, then when $i_{app} \approx 0.92$ all real parts go negative. So we expect only to find periodic solutions if $i_{app} \in (0.10, 0.92)$, roughly.

3.3 Results

The computations in this section begin to reveal the behaviour of the system of three coupled reciprocally inhibitory oscillators, but clearly do not present a complete picture. At best, they indicate that in "extreme" cases, the behaviour of this system can mimic that of *Emerita* during its dig. Specifically, with no bilateral coupling the three Morris-Lecar oscillators behave like the legs and uropod at the beginning of a dig, and the three symmetrically coupled oscillators mimic the end of the dig.

The high dimensionality of this system makes analysis very difficult, which is why only symmetric cases were treated. Dealing with these and similar equations it would be difficult or impossible to draw conclusions about the behaviour of the system when, say, the coupling between the legs is half or a quarter as strong as that between each leg and the uropod. Since the symmetric cases result in limit cycles corresponding to

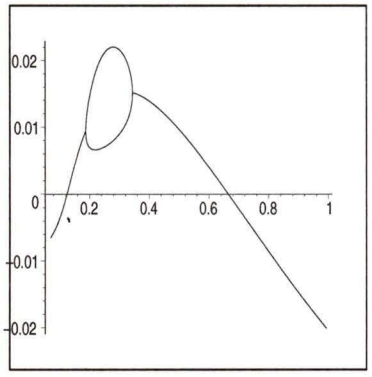

(a) Eigenvalues of A^* (real parts)

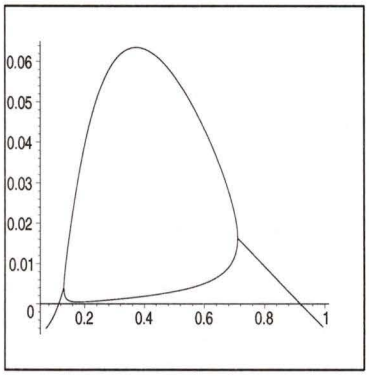

(b) Eigenvalues of B^* (real parts)

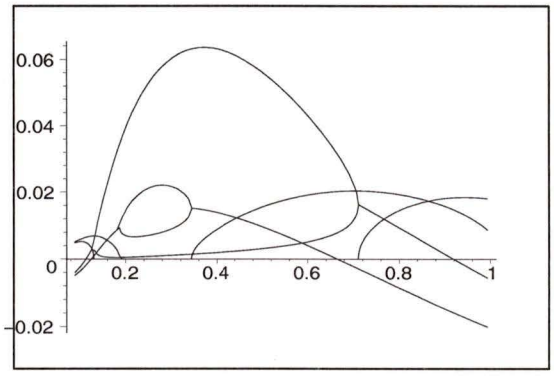

(c) Eigenvalues of M (both real parts (from (a) and (b)) and imaginary parts)

Figure 3.6: Plots of the eigenvalues of the linearization matrix in (3.2.4). In each plot, the vertical axis denotes the magnitudes of the real and imaginary parts of the indicated eigenvalues, and the horizontal axis is i_{app}. Hopf bifurcations occur when the real parts of the complex eigenvalues change sign.

the leg phases either at the beginning or at the end of a dig, a natural assumption is that over a range of bilateral coupling strengths there will exist limit cycles in which the phase differences between the appendages correspond to the leg phases at intermediate stages of a dig. Analysis of such systems requires that first the equations be simplified via averaging to a 3-dimensional system of phase equations.

Chapter 4

Reduction to Phase Equations by Averaging

Given that any oscillator described by an autonomous system of ordinary differential equations must be at least two-dimensional, it follows that even the simplest arrangement of (two) coupled oscillators must be at least four-dimensional. Clearly systems of n oscillators are at least $2n$-dimensional, and usually mn-dimensional where m is the dimension of each oscillator. The inherent high dimensionality of these systems of equations motivates the search for appropriate simplifications.

In the case of *Emerita*, the three oscillatory CPGs require at least six dimensions, and likely many more in order to account minimally for the observed behaviours. The special symmetry cases explored in the previous chapter were insufficient to account for the asymmetries in the data. The following equations for a cellular network permit the use of averaging techniques [1] [2] [17] [19] that dramatically reduce the important dimension of the system, thus simplifying the analysis.

Consider three oscillators all coupled together via inhibitory connections as in Figures 4.1(a) and (b), where the parameters a and b denote the strength of bilateral coupling. Both arrangements represent the same physical connections, but the

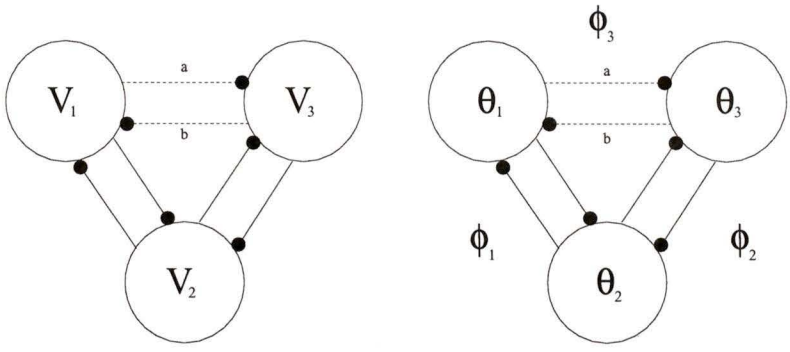

(a) CPGs represented by voltage equations

(b) CPGs represented by phase equations

Figure 4.1: Two ways to view the networks.

variables in each are different. In Figure 4.1(a), each oscillator is described by m variables, so the full system is $3m$-dimensional. In Figure 4.1(b), the three oscillators are assumed identical, or nearly identical, and each is described only by its phase, or distance along its limit cycle (θ). In fact, the important variable is the phase *difference* (ϕ) between adjacent oscillators. Either way, after reduction to angular variables, the network of CPGs is described by only three equations.

In Figure 4.1(a) equations describing the system are of the form

$$\frac{dV_i}{dt} = F(V_i) + g_{syn}G_i(V_1, V_2, V_3) \tag{4.0.1}$$

which is like (3.2.1) but with $V_i \in \mathbb{R}^m$, $i \in \{1, 2, 3\}$. The function F describes the intrinsic properties of each oscillator, and the functions G_i describe coupling between oscillators. The parameter $g_{syn} \ll 1$ makes the strength of the coupling small compared to the intrinsic properties of each oscillator. Equations describing Figure 4.1(b) are of the form

$$\frac{d\theta_i}{dt} = \omega_i + H_{i,i+1}(\theta_{i+1} - \theta_i) + H_{i,i+2}(\theta_{i+2} - \theta_i) \tag{4.0.2}$$

where $\theta_i \in \mathbb{S}^1$, $i \in \{1,2,3\}$ is taken mod 3, and ω_i is the intrinsic frequency of the oscillator. If the oscillators are identical, then $\omega_1 = \omega_2 = \omega_3$. If coupling functions are also identical, letting $\phi_i = \theta_{i+1} - \theta_i$ gives equations describing the phase *differences* between adjacent oscillators as

$$\frac{d\phi_i}{dt} = H_{i+1,i+2}(\phi_{i+1}) + H_{i+1,i}(-\phi_i) - H_{i,i+1}(\phi_i) - H_{i,i+2}(-\phi_{i+2}) \tag{4.0.3}$$

where $\phi_i \in \mathbb{S}^1$, $i \in \{1,2,3\}$, and $\phi_i = \phi_{i+3}$. Note that, since the oscillators are coupled in a ring, $\phi_1 + \phi_2 + \phi_3 = 2n\pi$ ($n \in \mathbb{Z}$). These phase equations (4.0.2) and (4.0.3) can be obtained from the original system (4.0.1) by averaging, which is often difficult and must be done numerically. Kopell, Ermentrout, and others [2] [11] [19] describe the averaging procedure clearly. The following example illustrates the procedure analytically, but subsequent computations of H functions will be numeric.

4.1 Illustration Using Simple Oscillators

As a very simple example of a reduction to phase equations for two coupled oscillators, consider the following two-dimensional system of equations, similar to the FitzHugh-Nagumo Oscillator, created for this illustration:

$$\begin{aligned} \frac{dx}{dt} &= x(1-x^2) - y \\ \frac{dy}{dt} &= x \end{aligned} \tag{4.1.1}$$

Its stable limit cycle is shown (computed numerically) in Figure 4.2. Qualitatively, this oscillator behaves like many of the other neural oscillators, but its simplicity permits analytical reduction to phase equations. The method involves two steps. First, the variables must be changed in such a way that, in the new system, one variable represents a phase, or distance along its intrinsic limit cycle, and the other

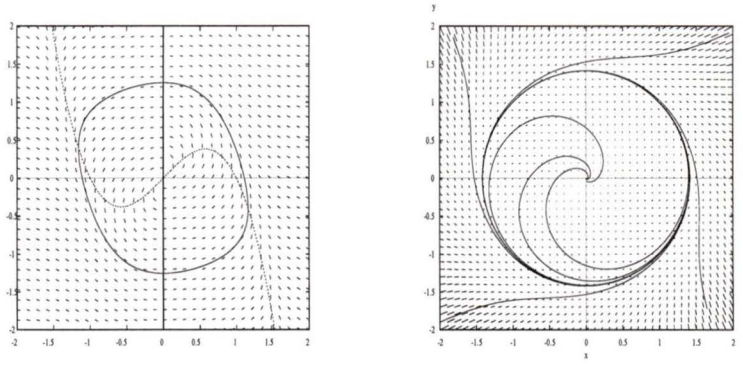

(a) Solution to (4.1.1) (b) Solution to (4.1.2)

Figure 4.2: Comparison between a simple FitzHugh-Nagumo-type oscillator (a) and a generic oscillator (b)

effectively describes how solutions approach the limit cycle. Second, the effect of one oscillator on the next must be averaged over a cycle, and the net effect written as a function of the phase difference between the oscillators. Let the smooth map

$$\mathcal{F}:\begin{bmatrix} u \\ v \end{bmatrix} \mapsto \begin{bmatrix} v(1-\sqrt{v^2+(-u-v^3+v)^2})-(-u-v^3+v) \\ \\ (-u-v^3+v)(1-\sqrt{v^2+(-u-v^3+v)^2})+v \end{bmatrix}$$

take the vector field of (4.1.1) to the vector field of equations

$$\begin{aligned} \frac{dx}{dt} &= x\left(1-\sqrt{x^2+y^2}\right)-y \\ \frac{dy}{dt} &= y\left(1-\sqrt{x^2+y^2}\right)+x. \end{aligned} \tag{4.1.2}$$

Using the obvious substitutions $r^2 = x^2+y^2$ and $\tan\theta = \frac{y}{x}$, equations (4.1.2) become

$$\begin{aligned} \frac{dr}{dt} &= r(1-r) \\ \frac{d\theta}{dt} &= 1 \end{aligned} \tag{4.1.3}$$

which clearly has the unit circle as a unique stable limit cycle.

Duplicating this system and introducing weakly inhibitory coupling between the x terms, the four dimensional system of two coupled oscillators is described by equations

$$\begin{aligned}
\frac{dx_1}{dt} &= x_1\left(1-\sqrt{x_1^2+y_1^2}\right) - y_1 - \varepsilon x_2 \\
\frac{dy_1}{dt} &= y_1\left(1-\sqrt{x_1^2+y_1^2}\right) + x_1 \\
\frac{dx_2}{dt} &= x_2\left(1-\sqrt{x_2^2+y_2^2}\right) - y_2 - \varepsilon x_1 \\
\frac{dy_2}{dt} &= y_2\left(1-\sqrt{x_2^2+y_2^2}\right) + x_2.
\end{aligned} \tag{4.1.4}$$

Numerical solution of this system quickly shows an apparent limit cycle as illustrated in Figure 4.3(a). Using the same substitutions as above,

$$\begin{aligned}
\frac{dr_1}{dt} &= r_1(1-r_1) - \varepsilon r_2 \cos\theta_1 \cos\theta_2 \\
\frac{d\theta_1}{dt} &= 1 + \frac{\varepsilon r_2}{r_1}\sin\theta_1 \cos\theta_2 \\
\frac{dr_2}{dt} &= r_2(1-r_2) - \varepsilon r_1 \cos\theta_2 \cos\theta_1 \\
\frac{d\theta_2}{dt} &= 1 + \frac{\varepsilon r_1}{r_2}\sin\theta_2 \cos\theta_1.
\end{aligned} \tag{4.1.5}$$

If the parameter ε were zero, then the two oscillators would operate independently, and the system would clearly have a stable limit cycle on $\mathbb{T}^2$, the torus comprising two unit circles. For ε small, this manifold is perturbed, but only slightly [6]. From (4.1.5), $\frac{dr_i}{dt} = 0$ when $r_i = 1 + O(\varepsilon)$. Substituting into the $\frac{d\theta_i}{dt}$ equations in (4.1.5) gives

$$\begin{aligned}
\frac{d\theta_1}{dt} &= 1 + \varepsilon \sin\theta_1 \cos\theta_2 + O(\varepsilon^2) \\
\frac{d\theta_2}{dt} &= 1 + \varepsilon \sin\theta_2 \cos\theta_1 + O(\varepsilon^2).
\end{aligned} \tag{4.1.6}$$

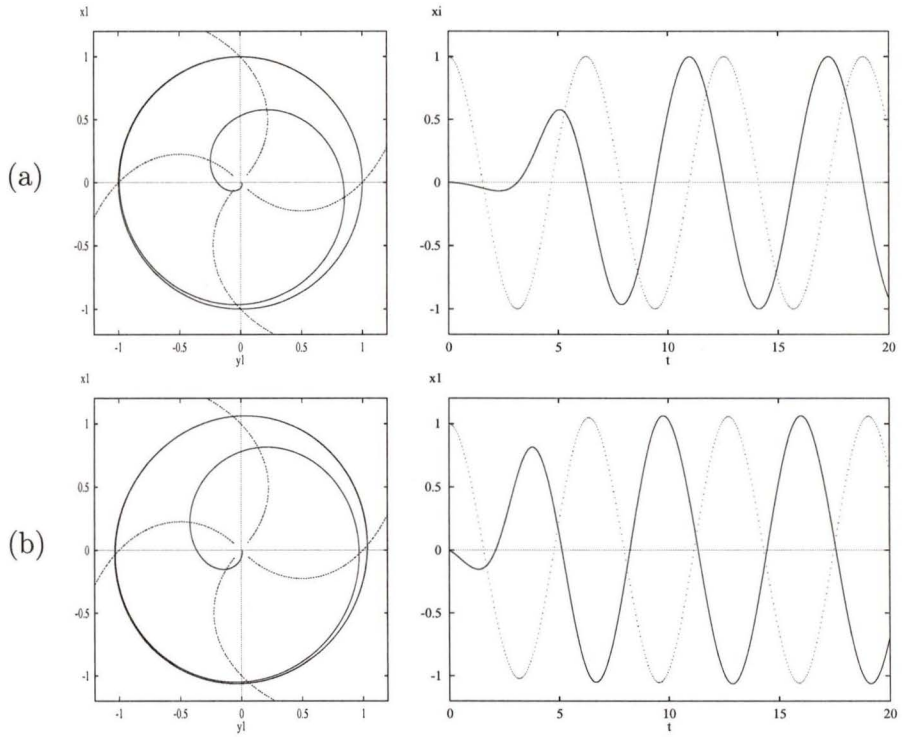

Figure 4.3: Some solutions to equations (4.1.4). In (a), $\varepsilon = 0$. In (b), $\varepsilon = 0.1$.

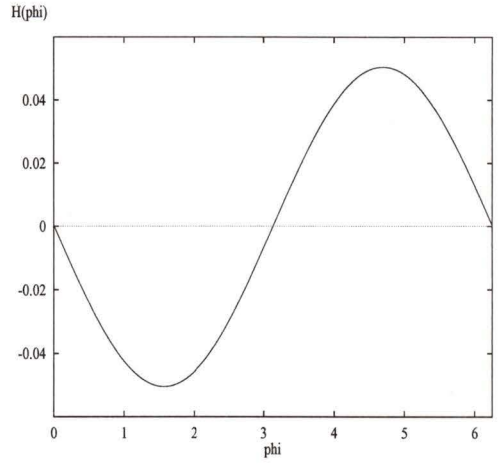

Figure 4.4: $H_{12}(\phi)$ computed numerically.

Letting $\phi \equiv \theta_2 - \theta_1$ be the phase difference between the two oscillators, (4.1.6) become

$$\begin{aligned} \frac{d\theta_1}{dt} &= 1 + \varepsilon \sin\theta_1 \cos(\phi + \theta_1) + O(\varepsilon^2) \\ \frac{d\theta_2}{dt} &= 1 + \varepsilon \sin\theta_2 \cos(\theta_2 - \phi) + O(\varepsilon^2). \end{aligned} \tag{4.1.7}$$

Finally, since the terms involving ϕ are small, their effects can be approximated by averaging over a cycle. Let

$$H_{12}(\phi) = \frac{1}{2\pi}\int_0^{2\pi} \varepsilon \sin\theta_1 \cos(\phi + \theta_1) d\theta_1 = -\frac{\varepsilon}{2}\sin\phi \tag{4.1.8}$$

$$H_{21}(-\phi) = \frac{1}{2\pi}\int_0^{2\pi} \varepsilon \sin\theta_2 \cos(\theta_2 - \phi) d\theta_2 = \frac{\varepsilon}{2}\sin(\phi). \tag{4.1.9}$$

Now, since $\phi = \theta_2 - \theta_1$,

$$\frac{d\phi}{dt} = H_{21}(-\phi) - H_{12}(\phi) = \varepsilon \sin\phi \tag{4.1.10}$$

which has $\phi = \pi$ and $\phi = 0$ as stable and unstable fixed points respectively.

Clearly, this is a cumbersome procedure depending on changing coordinates and is seldom likely to yield an explicit H function. Usually, these H functions are computed

using software. Figure 4.4, created using XPP shows the result of such a computation for the above example with $\varepsilon = 0.01$. Of course, it agrees with the function calculated above by direct averaging. Hereafter, all H functions will be computed using XPP and, where required, they will be approximated by the first several terms of their Fourier series, also computed numerically.

4.2 Application to a Cellular Network

Recall equation (4.0.1):

$$\frac{dV_i}{dt} = F(V_i) + g_{syn}G_i(V_1, V_2, V_3) \tag{4.2.1}$$

Using a system of Morris-Lecar equations as in Section 2.1.2 to describe each of the oscillators in Figure 4.1(a), and using simple sigmoidal coupling terms between oscillators as in Section 2.2,

$$\begin{aligned} F(V_i) &= \begin{bmatrix} g_l(v_l - v_i) + g_K n_i(v_K - v_i) + g_{Ca} m_\infty(v_i)(v_{Ca} - v_i) + i_{app} \\ \varphi\lambda_n(v_i)(n_\infty(v_i) - n_i) \end{bmatrix} \\ G_i(V_1, V_2, V_3) &= \begin{bmatrix} (S(v_{i+1}) + S(v_{i+2}))(v_{syn} - v_i) \\ 0 \end{bmatrix} \end{aligned} \tag{4.2.2}$$

where $V_i = \begin{bmatrix} v_i \\ n_i \end{bmatrix} \in \mathbb{R}^2$, $i \in \{1, 2, 3\}$, $v_{i+3} = v_i$, $n_{i+3} = n_i$, and $\lambda(v), n_\infty(v)$ and $m_\infty(v)$ are as in Section 2.1.2. The subscripts i correspond to the supscripts in Figure 4.1(a).

Uncoupled ($g_{syn} = 0$), each oscillator has a stable limit cycle as shown in Figure 4.5(a). For $0 < g_{syn} \ll 1$, the system, solved numerically with parameters as in Table 2.4, has a limit cycle in which the three oscillators remain close to their intrinsic

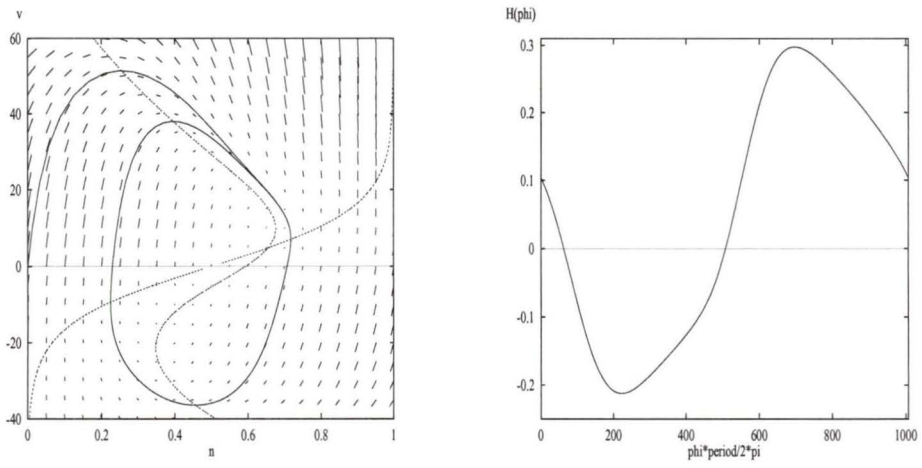

(a) Limit cycle and phase portrait

(b) Phase response curve

Figure 4.5: Limit cycle (a) and phase response curve (b) for a single Morris-Lecar neuron.

limit cycles, but are locked such that $\phi_i = \frac{2\pi}{3}, i \in \{1, 2, 3\}$, as indicated in Section 3.2. Showing this analytically is difficult, so the use of phase equations is necessary.

By symmetry, the H functions (Figure 4.5(b)) are identical between all oscillators. Since the oscillators are arranged in a ring, the sum of all the phase differences must be 2π. Making the substitution $\phi_2 = 2\pi - \phi_1 - \phi_3$, the system of phase equations (4.0.3) reduces further to

$$\begin{aligned} \frac{d\phi_1}{dt} &= H(-\phi_1 - \phi_3) + H(-\phi_1) - H(\phi_1) - H(-\phi_3) \\ \frac{d\phi_3}{dt} &= H(\phi_1) + H(-\phi_3) - H(\phi_3) - H(\phi_1 + \phi_3) \end{aligned} \tag{4.2.3}$$

Independent of the specific coupling functions, this system clearly has fixed points arising from symmetry when $\phi_i = 2n\pi$, or if $\phi_1 = \phi_3 = \frac{2\pi}{3}$. The location of other fixed points depends specifically on H. Numerical computation using Morris-Lecar equations with parameters as given in Table 2.4 yields the first ten Fourier coefficients

n	b_n	a_n
0	.049	0
1	.027	-.289
2	.007	.017
3	.004	.007
4	.004	.003

Table 4.1: First 10 Fourier Coefficients of $H(\phi)$ computed numerically from (4.2.2)

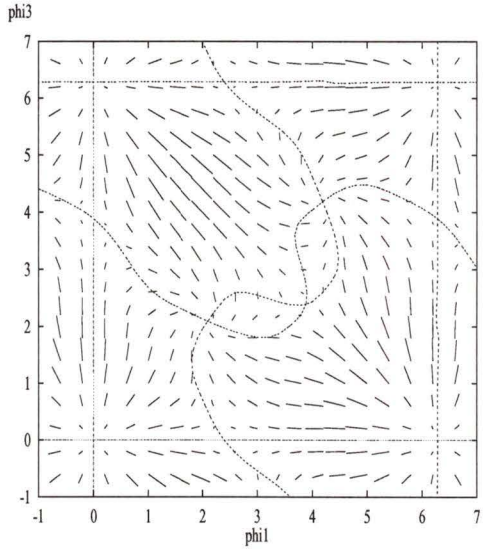

Figure 4.6: Vector Field of the $2D$ Phase equations (4.2.3).

of H, as listed in Table 4.1. These characterize the H-function, and the dominant terms will be used in approximations later.

Inspection of the vector field (Figure 4.6) suggests there should be six fixed points (at the intersections of the nullclines) on $\phi_1 \in [0, 2\pi)$, $\phi_3 \in [0, 2\pi)$, The origin is unstable, (0,3.89), (2.39, 0), and (3.89, 2.39) are saddles, and $(\frac{2\pi}{3}, \frac{2\pi}{3})$ and $(\frac{4\pi}{3}, \frac{4\pi}{3})$ are stable. These can easily be verified as fixed points, and linearization at each gives their stability.

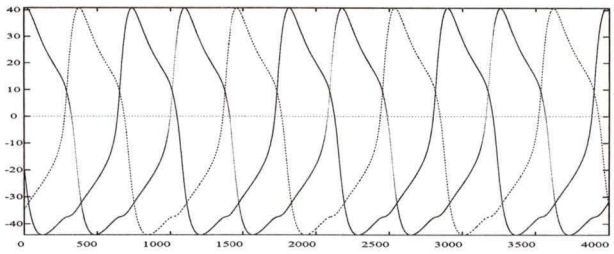

Figure 4.7: Numerical solution to (4.2.2)

Fixed points of the phase equation system correspond to limit cycles in the full system, though the phase system says nothing about the waveform of the oscillators [8]. Furthermore, their stability is preserved through the averaging procedure [17], so the *stable* fixed point in this system implies the existence of a *stable* limit cycle in the full system where the oscillators are locked with phase differences of $\frac{2\pi}{3}$. A numerical solution of the cellular equations (Figure 4.7) agrees with the solution of the phase equations.

So far, all three CPGs have been coupled identically and the results agree with those of Chapter 3. Clearly, the results are symmetric, and do not describe the digging data well. Adding multiplicative constants to the coupling terms in G_i in cellular equations provides a simple way to modulate the effects of neighbouring oscillators. To keep consistent with the bilateral symmetry of *Emerita*, coupling between the oscillators described by V_1 and V_3, or θ_1 and θ_3 must be targeted by symmetric connections in such a way that asymmetric phase differences can result from asymmetric stimuli. In the full $6D$ equations (4.2.1), G_2 is unchanged, but G_1

and G_3 become

$$\begin{aligned} G_1(V_1, V_2, V_3) &= \begin{bmatrix} g_{syn}(S(v_2) + bS(v_3))(v_{syn} - v_1) \\ 0 \end{bmatrix} \\ G_3(V_1, V_2, V_3) &= \begin{bmatrix} g_{syn}(aS(v_1) + S(v_2))(v_{syn} - v_3) \\ 0 \end{bmatrix} \end{aligned} \tag{4.2.4}$$

The parameters a and b, both non-negative, multiply the coupling terms between oscillators 1 and 3 as in Figure 4.1(b) so the phase equations become

$$\begin{aligned} \frac{d\phi_1}{dt} &= H(\phi_2) + H(-\phi_1) - H(\phi_1) - bH(-\phi_3) \\ \frac{d\phi_2}{dt} &= aH(\phi_3) + H(-\phi_2) - H(\phi_2) - H(-\phi_1) \\ \frac{d\phi_3}{dt} &= H(\phi_1) + bH(-\phi_3) - aH(\phi_3) - H(-\phi_2). \end{aligned} \tag{4.2.5}$$

or

$$\begin{aligned} \frac{d\phi_1}{dt} &= H(-\phi_1 - \phi_3) + H(-\phi_1) - H(\phi_1) - bH(-\phi_3) \\ \frac{d\phi_3}{dt} &= H(\phi_1) + bH(-\phi_3) - aH(\phi_3) - H(\phi_1 + \phi_3) \end{aligned} \tag{4.2.6}$$

where all H functions are identical. It is the asymmetry in the parameters a and b that destroys the symmetry of the whole system.

Clearly, with $a = b = 1$, coupling is symmetric, and equations (4.2.3) are recaptured, but now there is freedom to modify the strength of the coupling between oscillators 1 and 3 independently. Increasing a increases the inhibitory effect that oscillator 1 has on oscillator 3. Likewise, increasing b increases the inhibitory effect that oscillator 3 has on oscillator 1. If both a and b are zero, it is as though cells 1 and 3 are not connected. The intermediate parameter values begin to account for some of the phase differences seen in the digging data. For example, if $a = 0$ and

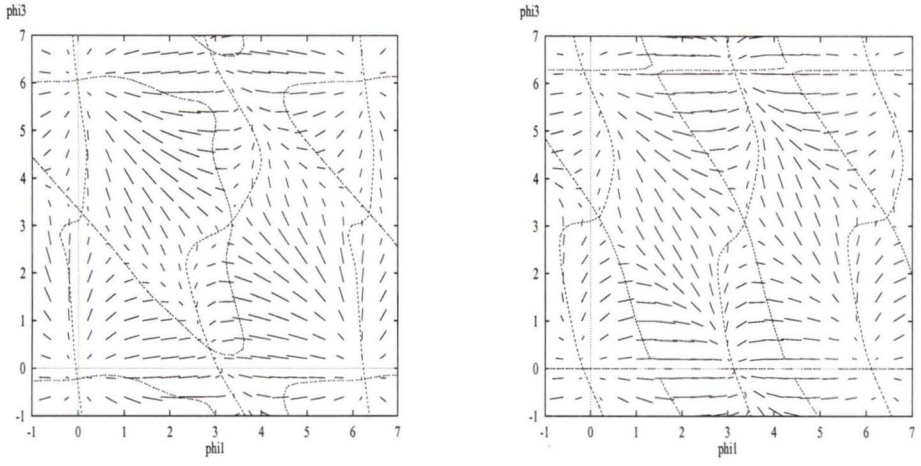

(a) (b)

Figure 4.8: Vector Field of (4.2.6) if (a) $a = 0, b = .7$ or (b) $a = b = 0$

$b = 0.7$, using $H(\phi)$ as shown in Figure 4.5, numerical solution of (4.2.6) gives the vector fields in Figure 4.8.

Qualitatively, this vector field is similar to Figure 4.6, but it shows that some of the fixed points have migrated, and two have vanished. Here, the fixed point $(\phi_1, \phi_3) \cong (3, 0.5)$ has shifted from $(\phi_1, \phi_3) = (\frac{2\pi}{3}, \frac{2\pi}{3})$. The location of these fixed points changes continuously with continuous changes in the parameters a and b.

For some simple H functions, the movement of the fixed points can be tracked analytically, but usually, they must be tracked numerically. Figure 4.9 shows how the fixed points migrate as a or b are varied using the first 10 Fourier coefficients of the H function depicted in Figure 4.5(b) and Table 4.1. Note that as either a or b increases from zero, with the other fixed at zero, the legs are driven further out of phase with each other. Also note that as a increases, ϕ_3 decreases, so the right leg starts to lead. Conversely, as b increases, the left leg starts to lead. The specific behaviour will be

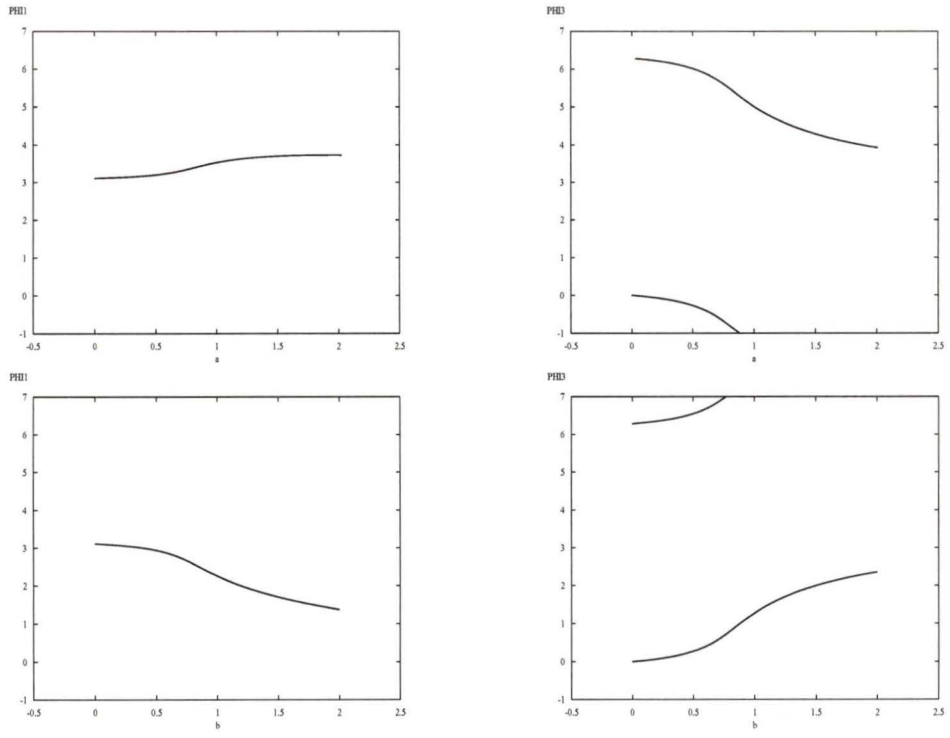

Figure 4.9: Equilibrium phases as they depend on the parameters a and b.

discussed in more detail in the next section.

4.3 Tracking the Fixed Points

The locations of the fixed points of the phase equations determine the stable phase relationships of the CPGs. Therefore, understanding how the coupling parameters affect the phase relationships requires tracking these points. Recall the example described by equations (4.1.1) leading to the computation of $H(\phi) = \frac{-\varepsilon}{2} \sin\phi$ in (4.1.8).

Substituting this H into (4.2.5) gives a 3-oscillator system

$$\begin{aligned} 2\frac{d\phi_1}{dt} &= -\varepsilon\sin(\phi_2) + 2\varepsilon\sin(\phi_1) - b\varepsilon\sin(\phi_3) \\ 2\frac{d\phi_2}{dt} &= -a\varepsilon\sin(\phi_3) + 2\varepsilon\sin(\phi_2) - \varepsilon\sin(\phi_1) \\ 2\frac{d\phi_3}{dt} &= -\varepsilon\sin(\phi_1) + (a+b)\varepsilon\sin(\phi_3) - \varepsilon\sin(\phi_2) \end{aligned} \tag{4.3.1}$$

Setting $\frac{d\phi_i}{dt}$ equal to zero in (4.3.1) to find fixed points, and eliminating ϕ_2 from the first two equations gives

$$\sin(\phi_1) = \frac{a+2b}{3}\sin(\phi_3) \tag{4.3.2}$$

Note that if $a = b = 0$, the three oscillators are effectively arranged in a chain, and $\sin(\phi_1) = \sin(\phi_2) = 0$. This gives the fixed points $(\phi_1, \phi_2) = (m\pi, n\pi)$. To find others, assume that not both a and b are zero.

From the $\frac{d\phi_1}{dt}$ equation, since $\phi_2 = 2\pi - \phi_1 - \phi_3$, $\sin\phi_2$ can be expanded in terms of ϕ_1 and ϕ_3 so that, at a fixed point,

$$0 = \sin(\phi_3)\left[\frac{a+2b}{3}\cos(\phi_3) + \cos(\phi_1) + 2\frac{a+2b}{3} - b\right]$$

So $\phi_3 = n\pi$, or

$$-\cos(\phi_1) = \frac{a+2b}{3}\cos(\phi_3) + 2\frac{a+2b}{3} - b \tag{4.3.3}$$

Squaring both sides, applying the fundamental trigonometric identity to the left hand side, and simplifying gives

$$\cos(\phi_3) = \frac{9 - (a+2b)^2 - (2a+b)^2}{2(2a+b)(a+2b)} \tag{4.3.4}$$

Similar calculations show that at equilibria, $\phi_1 = n\pi$ or

$$\cos(\phi_1) = \frac{(a+2b)^2 - (2a+b)^2 - 9}{6(2a+b)} = \frac{(b^2-a^2) - 3}{2(2a+b)}. \tag{4.3.5}$$

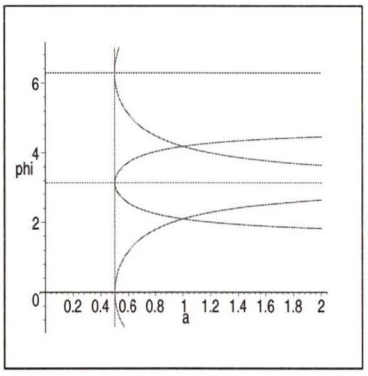

Figure 4.10: Bifurcations of equilibrium phases for $H(\phi) = -\sin\phi$.

It follows that $\phi_2 = n\pi$ or

$$\cos(\phi_2) = \frac{(2a+b)^2 - (a+2b)^2 - 9}{6(a+2b)} = \frac{(a^2-b^2)-3}{2(a+2b)}. \tag{4.3.6}$$

These equations give equilibrium surfaces over the parameters a and b. Fixing either parameter at zero and varying the other gives a section of the surface as in Figure 4.10.

There is clear symmetry in these equations, and redundancy since any two equilibrium phases imply the third. To simplify the analysis, it is useful to study the system

$$\begin{aligned} \frac{d\phi_1}{dt} &= 0 = \varepsilon\sin(\phi_1+\phi_3) + 2\varepsilon\sin(\phi_1) - b\varepsilon\sin(\phi_3) \\ \frac{d\phi_3}{dt} &= 0 = -\varepsilon\sin(\phi_1) + (a+b)\varepsilon\sin(\phi_3) + \varepsilon\sin(\phi_1+\phi_3). \end{aligned} \tag{4.3.7}$$

Letting $b = 0$, and varying a (or vice-versa) gives pitchfork bifurcations (as shown in Figure 4.10) in both phase variables when the coupling parameter $a = 0.5$ (or $b = 0.5$ if $a = 0$). Clearly, the loci of equilibria shown in Figures 4.9 and 4.10 appear very different. The fact that, in this example, H is an odd function of ϕ imposes an artificial symmetry on the system. If H is odd, then there are equilibria when $\phi_i = n\pi$. If H is perturbed slightly, some of these equilibria vanish, leaving

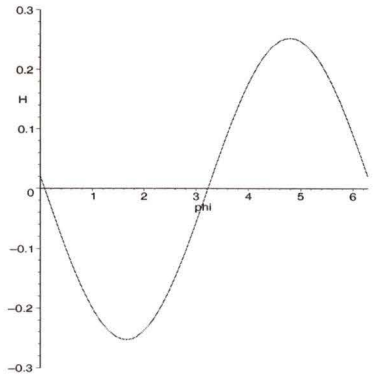

Figure 4.11: Single term approximation to H

only one stable branch of the pitchfork. By comparison to the H function computed numerically for the Morris-Lecar system (Figure 4.5), a more accurate simplification is to approximate it using the two dominant terms in the Fourier series, which can be combined into one. Figure 4.11 shows a comparison of the H functions computed for the Morris-Lecar oscillator using only two Fourier coefficients.

Letting $H(\phi) = .027\cos\phi - .289\sin\phi = -0.29\sin(\phi - 0.1)$, the sum of the first two nonconstant Fourier series terms, the bifurcation picture changes appropriately, and it is clear that as either a or b is increased from zero with the other fixed, the phases of the left and right legs are driven apart. Figure 4.12 shows the effects of varying the parameters.

The coupling parameters have the most direct effect on ϕ_3, representing the phase difference between the right and left legs. The variables ϕ_1 and ϕ_2 are equivalent up to symmetry, and both feel the effects of the parameter changes less directly. Whatever effect a has on ϕ_1, b has on ϕ_2 and vice-versa. The effect of increasing either parameter is to drive the legs out of phase with each other while advancing one and retarding the other with respect to the uropods. Increasing a causes the

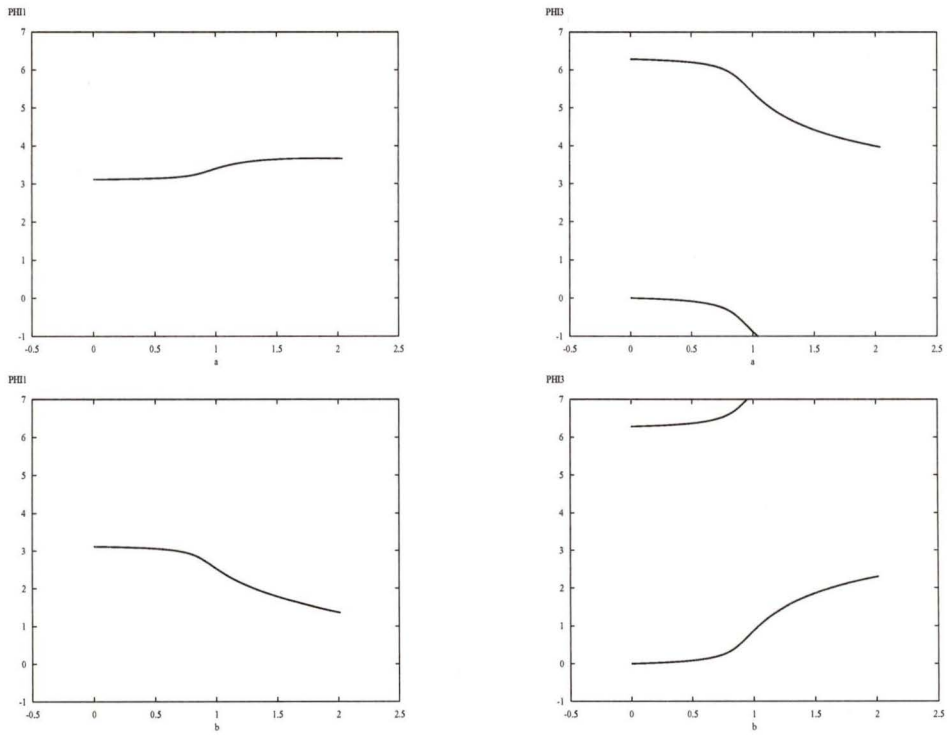

Figure 4.12: Equilibrium plots for the simplified H function

right leg to lead while increasing b causes the left to lead. These phase relationships are consistent with those in the data. However, excitatory bilateral connections are possible physiologically. Since these CPGs do not allow for the possibility of excitatory connections, it is clear that the they are too simple, and elaborations are necessary.

Assuming that choosing Morris-Lecar equations to describe the complete CPGs gives, at best, a qualitative approximation to the real observed behaviour, it is imperative that the results are robust to perturbations of the H functions. Choosing $H(\phi) = -A\sin(\phi - \alpha)$, where A and α are positive constants, results numerically in equilibrium plots similar to those of Figure 4.9 over a reasonable range of α values. It is apparent that introducing the parameter α destroys the artificial symmetry imposed by the selection of an odd H function, and enables the phase model to reproduce the data. As α tends to 0, the bifurcation picture tends to the one shown in Figure 4.10. In a very coarse sense, the behaviour of the interaction of three neurons described by Morris-Lecar equations can be approximated by the behaviour of three arbitrary oscillators coupled by equations of the form $H(\phi) = -A\sin(\phi - \alpha)$. The parameters regulate the strength of coupling in such a way that, with minimal sensory input, the system (symmetric except for the values of a and b) can produce the asymmetric output observed in the lab.

Chapter 5

Coupled CPG Model

Recall from the Introduction that each CPG controlling one of *Emerita's* appendages likely contains on the order of 30-70 neurons. It would be ludicrous to try to construct an ODE model to describe each in detail, but it is likely that to describe each CPG by a single Morris-Lecar neuron is an oversimplification. Building on the systems presented in Chapter 3 compounds the difficulty in analysis. However, numerical computation of H functions followed by subsequent analysis of the resulting phase equations, as in Chapter 4, works to reduce even higher dimensional systems (using more complex CPGs) to three dimensions.

In this chapter, models will be constructed of varying complexity based on models of crayfish CPGs proposed by Skinner and others [29] [30]. Reduction to phase equations will be used as a mechanism by which it can be concluded that in *Emerita*, as long as all of the CPGs are similar, simply varying the coupling strength between those controlling the legs is sufficient to model their digging behaviour.

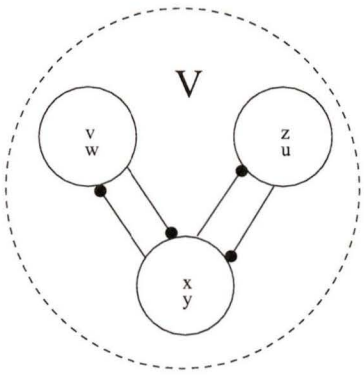

Figure 5.1: CPG comprising three neurons

5.1 3-Neuron CPGs with Sigmoidal Coupling

According to previous work (see [21] [29]) the CPGs responsible for coordinating the movement of crayfish swimmerets contain many cells that can be grouped into at least three distinct populations. Suppose, due to phylogeny, that the same can be assumed for *Emerita*. Instead of modelling each CPG as a single oscillator, if each of these *populations* is modelled as an oscillator, then each CPG can be modelled as a system of three oscillators (depicted in Figure 5.1) each of which can be described by a Morris-Lecar system. In this case, each CPG is still modelled by equations of the form

$$\frac{dV_i}{dt} = F(V_i) \tag{5.1.1}$$

but now $V_i \in \mathbb{R}^6$ and the coupling between neurons contained within the CPG is accounted for in the F function. Figure 5.2 shows an arrangement in which three such CPGs are coupled symmetrically in a way that is similar to the network of Section 3.2. If connections between each are via the qualitative sigmoidal functions described in Section 2.4, then the above network comprises 9 two-dimensional neurons

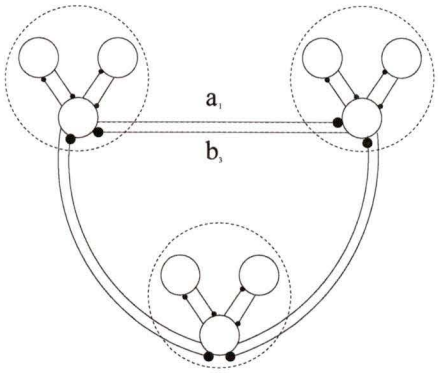

Figure 5.2: Three CPGs with variable bilateral coupling

and is described on $\mathbb{R}^{18}$ by equations of the form

$$\frac{dV_i}{dt} = F(V_i) + G_i(V_1, V_2, V_3) + I_{app} \tag{5.1.2}$$

where $i \in \{1, 2, 3\}$, but where $V_i = \begin{bmatrix} v_i \\ w_i \\ x_i \\ y_i \\ z_i \\ u_i \end{bmatrix}$ and I_{app} is a vector of applied currents.

Note that, for convenience in notation, the variables w_i replace the variables n_i from Chapter 3. Again, the functions F_i describe the intrinsic properties of the CPG, and the functions G_i describe the connections between CPGs. So, to describe Figure 5.2,

$$F(V_i) = \begin{bmatrix} g_l(v_l - v_i) + g_K w_i(v_K - v_i) + g_{Ca} m_\infty(v_i)(v_{Ca} - v_i) + g_{syn} S(x_i)(v_{syn} - v_i) \\ \varphi\lambda(v_i)(S(v_i) - w_i) \\ g_l(v_l - x_i) + g_K y_i(v_K - x_i) + g_{Ca} m_\infty(x_i)(v_{Ca} - x_i) + g_{syn}(S(v_i) + S(z_i))(v_{syn} - x_i) \\ \varphi\lambda(x_i)(S(x_i) - y_i) \\ g_l(v_l - z_i) + g_K u_i(v_K - z_i) + g_{Ca} m_\infty(z_i)(v_{Ca} - z_i) + g_{syn} S(x_i)(v_{syn} - z_i) \\ \varphi\lambda(z_i)(S(z_i) - u_i) \end{bmatrix}$$

and

$$G_i(V_1, V_2, V_3) = \begin{bmatrix} 0 \\ 0 \\ g_{syn}(a_i S(x_{i-1}) + b_i S(x_{i+1}))(v_{syn} - x_i) \\ 0 \\ 0 \\ 0 \end{bmatrix}$$

where $i \in \{1, 2, 3\}$ is taken mod 3, $S(v)$ is the sigmoid function described in Section 2.2, and all parameters and functions are as defined in Table 2.4 and Section 2.1.2. The constants a_i and b_i determine the strength of coupling between CPGs and, unless stated otherwise, have a value of 0.1 to ensure that coupling between CPGs is weak compared to the intrinsic properties of each. The variables v, x and z represent the voltages of individual cells and the variables w, y and u represent their respective ion channel dynamics.

Despite the fact that this system is substantially more complex than (4.2.1), numerical solutions and H functions are still easy to obtain with XPP. Figure 5.3 shows some such solutions with parameters as given in Table 3.1 and in the figure captions. Notice that the bilateral coupling parameters at least appear to have an effect here similar to the effect they had in Chapters 3 and 4. In order to understand the effect of the bilateral coupling parameters better, it is necessary again to reduce the dimension of the system.

Using (5.1.2) to describe the intrinsic oscillation of a CPG, the H functions describing connections between CPGs are computed numerically as in Chapter 4. Figure 5.4(a) shows such an H function for inhibitory coupling between x_i variables as in Figure 5.2. The first ten Fourier coefficients of H are listed in Table 5.1, and Fig-

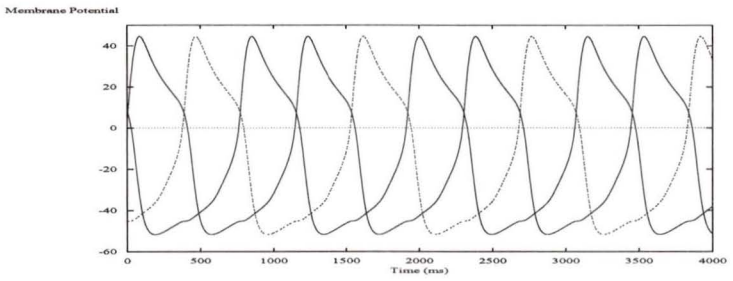

(a) $a_1 = b_3 = 1$

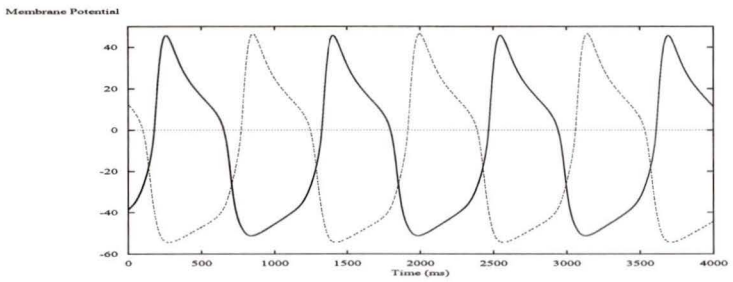

(b) $a_1 = b_3 = 0$

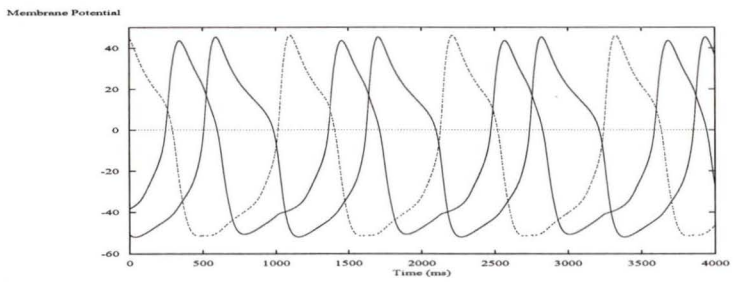

(c) $a_1 = 1$, $b_3 = 0$

Figure 5.3: Some numerical solutions to (5.1.2). Parameters are as given in Table 2.4 with $i = 0.4$. Coupling parameters are indicated.

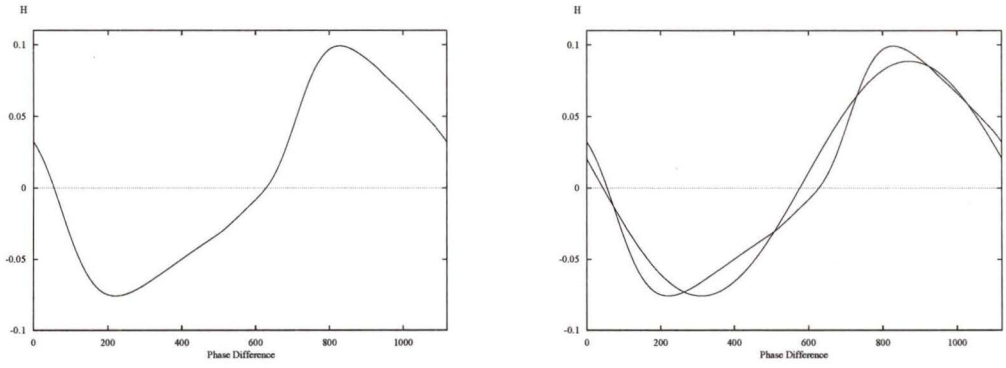

(a) Ten term approximation

(b) Ten and two term approximations

Figure 5.4: H functions for (5.1.2) computed numerically

n	b_n	a_n
0	.0052	0
1	.0282	-.0447
2	.0009	-.0086
3	.0004	.0044
4	.0032	.0014

Table 5.1: First 10 Fourier Coefficients of $H(\phi)$ computed numerically from (5.1.2)

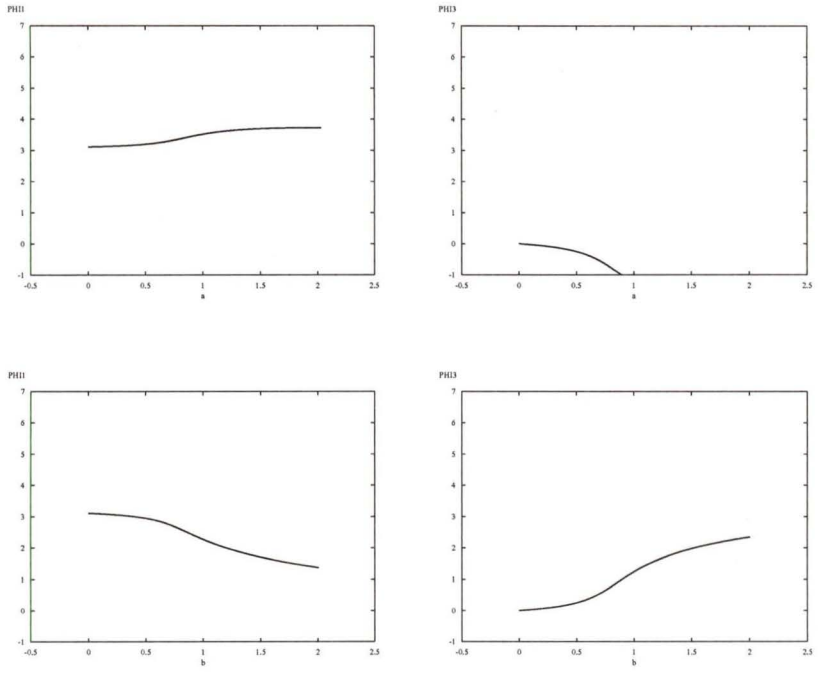

Figure 5.5: Equilibrium values of (5.1.3) as they depend on coupling parameters

ure 5.4(b) shows an approximation to H qualitatively similar to that in Figure 4.5. Using the first two nonconstant terms of the Fourier series, H can be written as $H(\phi) = -A\sin(\phi - \alpha)$, so the full network is described as in (4.2.5) and (4.2.6) Using, in this case, $H(\phi) = -0.05285\sin(\phi - 0.56)$, AUTO tracks the fixed points numerically. Figure 5.5 shows how the equilibrium values of the phase variables ϕ_1 and ϕ_3 vary with the coupling parameters a and b. In each of the plots, one of the parameters is fixed at zero while the other is varied as indicated.

With this more elaborate network, there are other ways to connect the CPGs. In the preceding arrangement, the cells described by x_i and y_i within each CPG were coupled via inhibitory connections. Changing the sign of v_{syn} makes the connections

excitatory, generating very different results. Taking v_{syn} to be, say, 70 effectively flips the H function about the x-axis. The result, computed numerically, is a limit cycle in which all three oscillators follow very similar trajectories for any values of a or b.

Given that the network should be bilaterally symmetric, there are eight unique ways to connect the CPGs associated with the legs. Figure 5.6 shows each, together with its bilateral H function, and numerical solutions to each system.

From the numerical solutions, it is apparent that the limit cycles shown in Figure 5.6(c-f) could possibly model the behaviour, while those shown in Figure 5.6(a, b, g, h) could not. Indeed, equilibrium plots generated as in Chapter 4 are qualitatively similar whenever $H(\phi)$ is qualitatively similar to that in Figure 5.4.

Though these results seem reasonable, they are unsatisfactory in that connections between CPGs are modelled as non-spiking interneurons. The final elaboration is to add in spiking interneurons between spatially distinct CPGs.

5.2 3-Neuron CPGs Connected by Spiking Interneurons

Take, now, the coupling between CPGs to be via FitzHugh-Nagumo neurons, where synapses between the target cells and the FitzHugh-Nagumo cells are described by the ODEs outlined in Section 2.2. Figure 5.8 illustrates an oscillator for which V_i, F_i

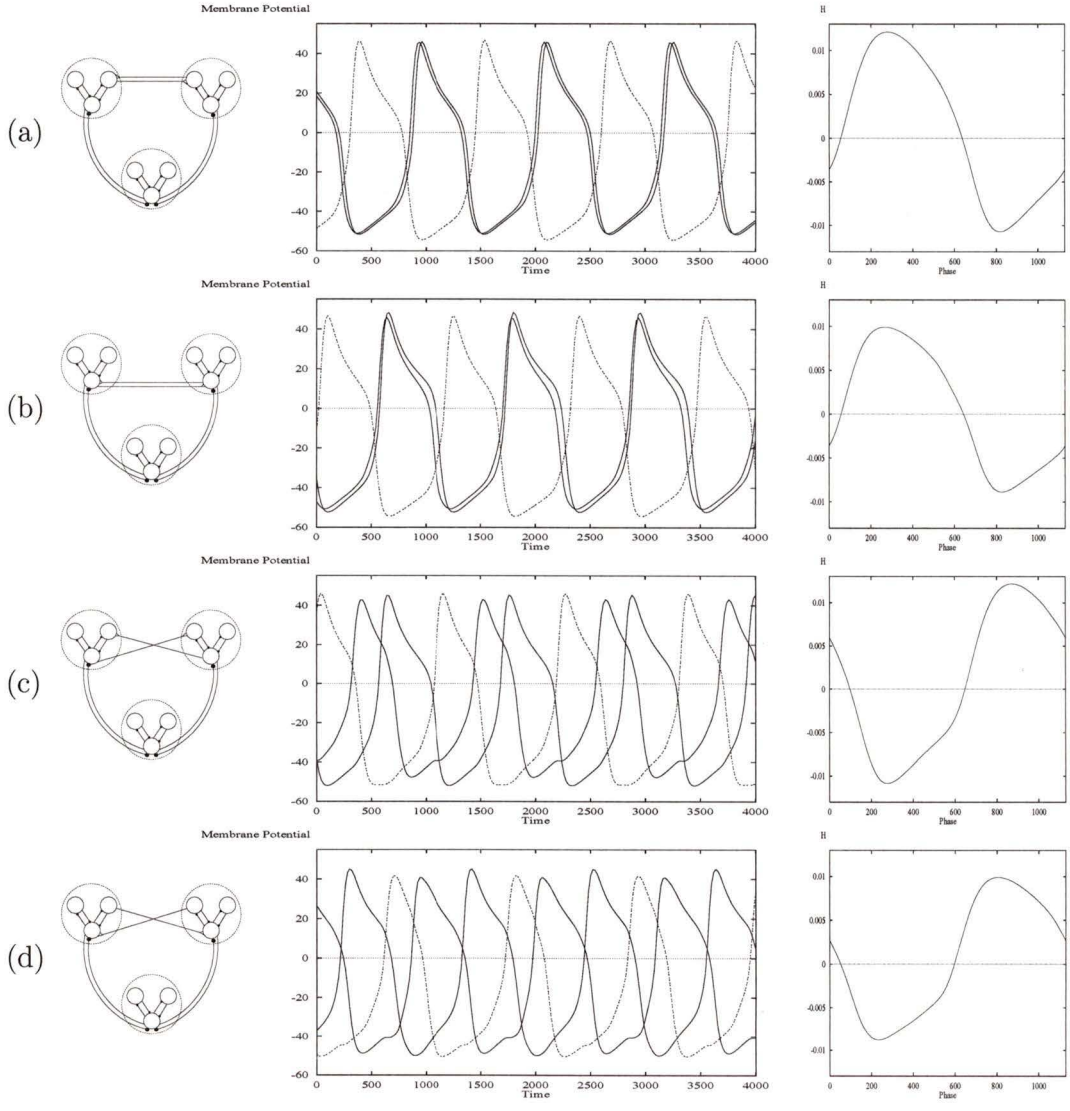
(a)
(b)
(c)
(d)
Membrane Potential
Time
H
Phase

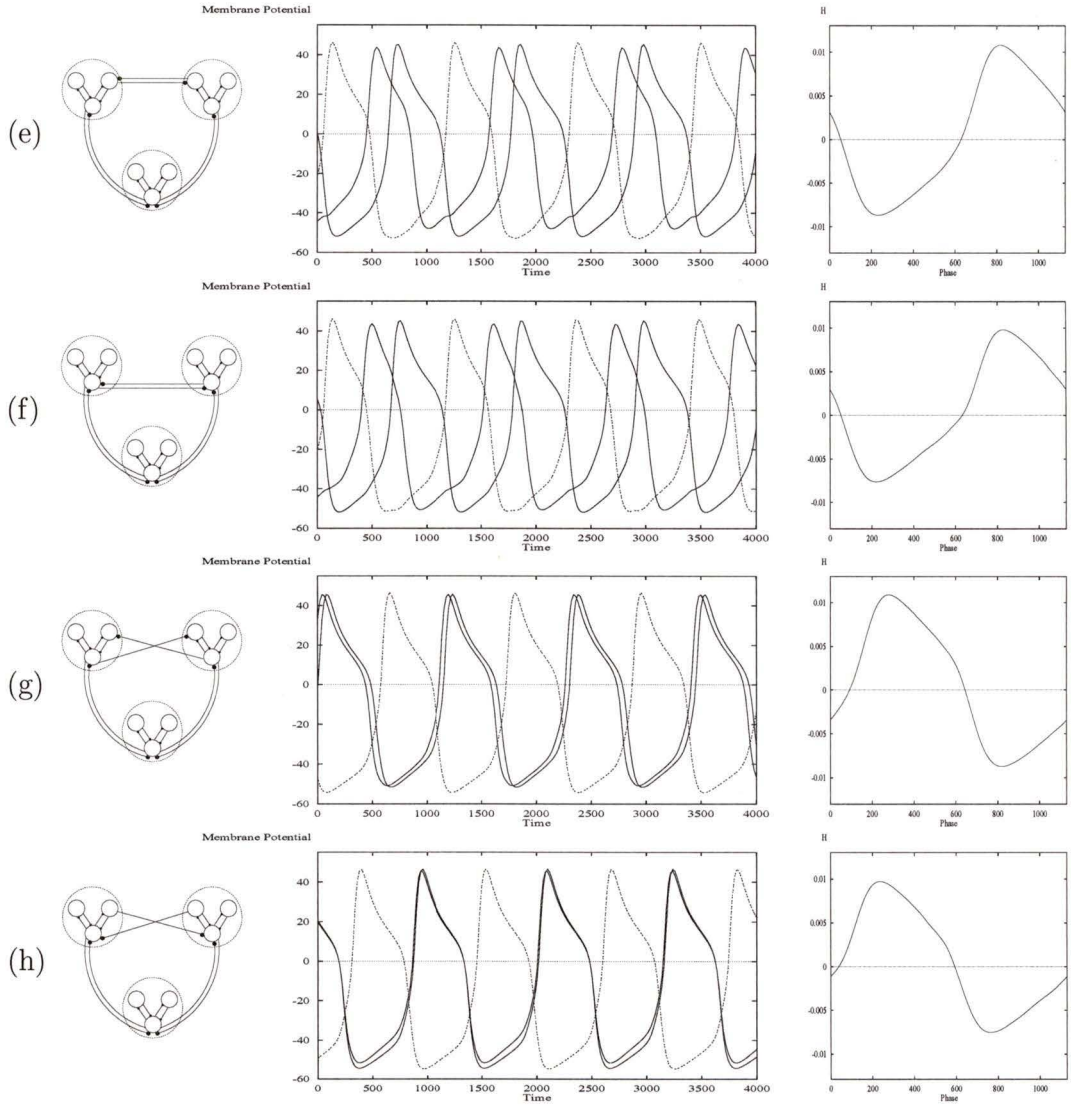

Figure 5.6: The possible bilateral connection patterns for 3-neuron CPGs together with their limit cycles and H functions.

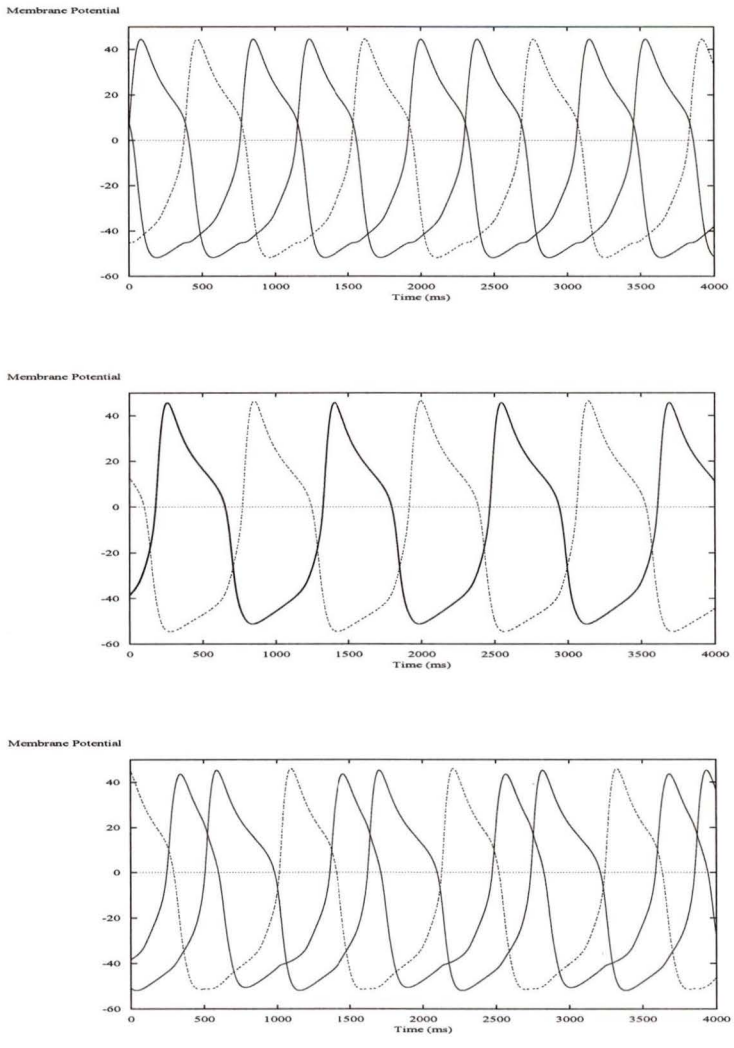

Figure 5.7: Numerical solutions to (5.1.2) with (a) $a = b = 1$, (b) $a = b = 0$, and (c) $a = 1, b = 0$.

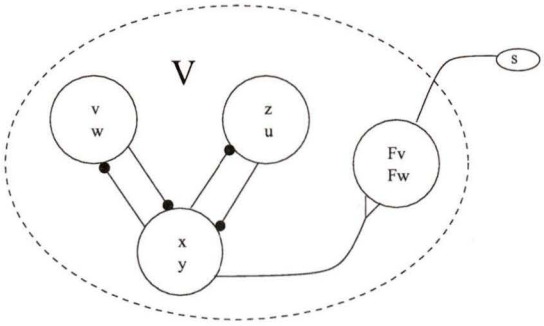

Figure 5.8: Schematic of a CPG comprising three Morris-Lecar neurons, one Fitz-Hugh-Nagumo neuron, and a synaptic differential equation.

and G_i are defined on $\mathbb{R}^9$. The right hand sides of (5.1.2) take the form

$$F(V_i) = \begin{bmatrix} g_l(v_l - v_i) + g_K w_i(v_K - v_i) + g_{Ca} m_\infty(v_i)(v_{Ca} - v_i) + g_{syn} S(x_i)(v_{syn} - v_i) \\ \varphi\lambda(v_i)(S(v_i) - w_i) \\ g_l(v_l - x_i) + g_K y_i(v_K - x_i) + g_{Ca} m_\infty(x_i)(v_{Ca} - x_i) + g_{syn}(S(v_i) + S(z_i))(v_{syn} - x_i) \\ \varphi\lambda(x_i)(S(x_i) - y_i) \\ g_l(v_l - z_i) + g_K u_i(v_K - z_i) + g_{Ca} m_\infty(z_i)(v_{Ca} - z_i) + g_{syn} S(x_i)(v_{syn} - z_i) \\ \varphi\lambda(z_i)(S(z_i) - u_i) \\ \frac{1}{\varepsilon}\left(5 \times 10^5 Fv_i(Fv_i + 30)(40 - Fv_i) - Fn_i + g_{syn} S(x_i)(80 - Fv_i)\right) \\ \frac{1}{60}(Fv_i - 5Fn_i + 15) \\ \frac{1}{\tau}\frac{s_\infty - s}{1 - s_\infty}. \end{bmatrix}$$

$$G_i(V_1, V_2, V_3) = \begin{bmatrix} 0 \\ 0 \\ g_{syn}(a_i s(x_{i-1}) + b_i s(x_{i+1}))(v_{syn} - x_i) \\ 0 \\ 0 \\ 0 \\ 0 \\ 0 \\ 0 \end{bmatrix} \tag{5.2.1}$$

where the functions s_i satisfy the differential equations given in Section 2.2. Figure 5.7 shows some numerical solutions to this system.

From Figure 5.8, it is clear that each CPG includes three Morris-Lecar neurons, a FitzHugh-Nagumo spiking neuron, and a DE to describe the synapse, making the full network (of 3 oscillators) 27 dimensional. Still, considering each CPG a 9-dimensional oscillator, the previous procedures permit the reduction of this system to a system of phase equations on $\mathbb{T}^3$. Figure 5.9 show various coupling arrangements together with numerical solutions and H functions. Note that these numerical results indicate that using this more complex system yields similar results to that of the lower dimensional system (4.2.2) of Chapter 4. For the sake of illustration, and comparison, Figure 5.10 shows how the equilibrium phases depend on the coupling parameters.

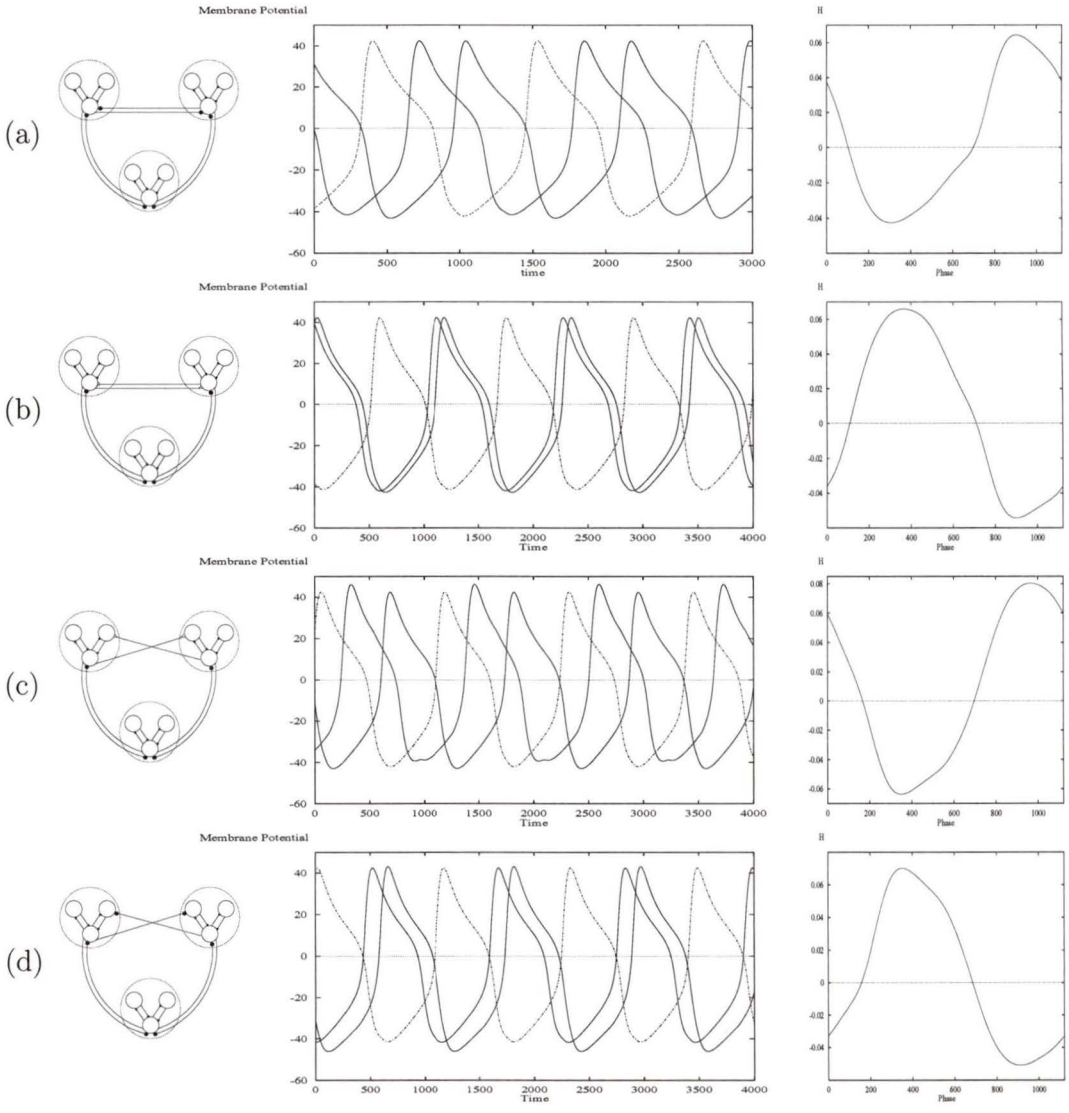

Figure 5.9: Some possible results of coupling oscillators. Reciprocal coupling is (a) inhibitory and (b) excitatory. Coupling from x to v or z variables is (c) excitatory and (d) inhibitory.

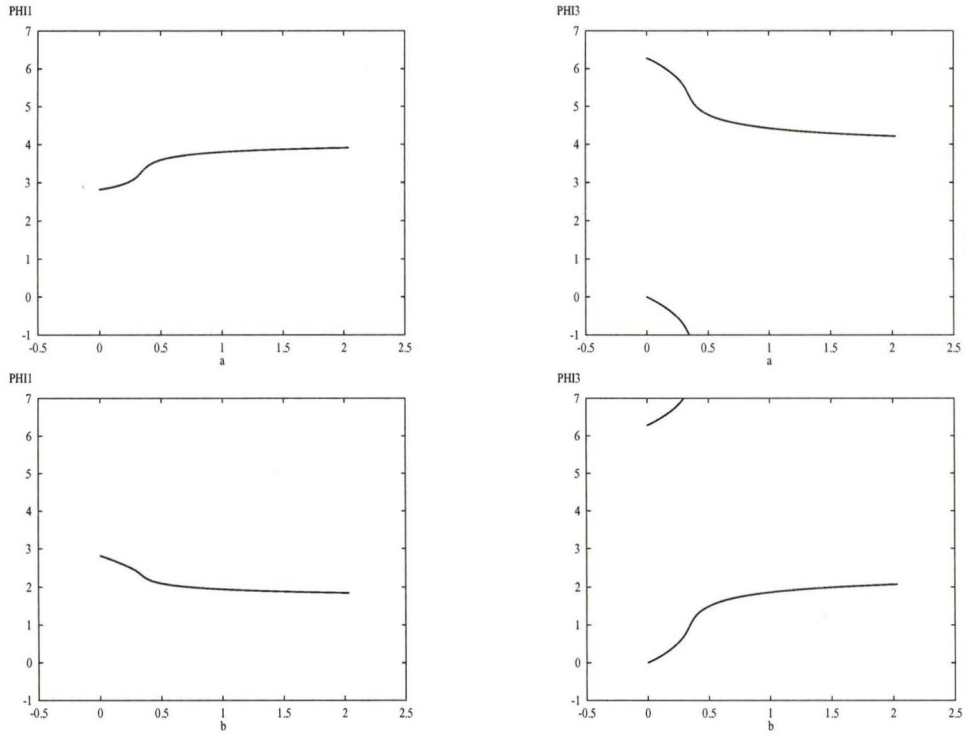

Figure 5.10: Equilibrium plots showing the result of bilateral reciprocal inhibition between x variables with coupling via a FitzHugh-Nagumo interneuron.

Chapter 6

Conclusion

Chapters 3, 4 and 5 all describe apparently different systems of equations with very similar results. Whether by numerical analysis or reduction to phase equations with subsequent analysis, it is clear that simply modifying the coupling between the legs is sufficient to reproduce the phase differences seen in the data for various neural arrangements.

Because each CPG is known to comprise many neurons, it is necessary to make simplifying assumptions for these models. Both the "coupled cell" and the "coupled CPG" models appear to reproduce much of the digging behaviour well, but it is clear that the coupled CPG model offers more flexibility in bilateral coupling arrangements. Using FitzHugh-Nagumo interneurons to connect the CPGs is likely more accurate than using the sigmoid approximations, but the resulting phase equations are similar. Therefore, the resulting behaviour is similar. I propose that the minimal model that can describe *Emerita*'s digging behaviour with sufficient flexibility to accommodate our lack of knowledge about the true nature of the bilateral coupling is the one formulated in Section 5.1.

The CPGs themselves were always considered identical (with the same frequency),

so the observation that for every cycle of the legs there is exactly one cycle of the uropods is accounted for immediately. One of the more interesting aspects of the behaviour is that the legs never cycle in phase with the uropods. Explaining this in terms of the models presented also relies on the CPGs having identical frequencies. In each model, the coupling between legs and uropods has been inhibitory, causing them to push apart. So, when there is no bilateral coupling between the legs, both cycle exactly out of phase with the uropods. In this arrangement, the only way to decrease the magnitude of the phase difference between the uropods and either leg is to force the legs apart. Since the legs (also inhibiting each other) cannot be more than π out of phase with each other, neither can be forced in phase with the uropod.

From the results of Chapters 4 and 5, it seems that a bilateral H function that is qualitatively similar to $H(\phi) = -\sin(\phi - \alpha)$ results in the appropriate behaviour, at least for $0 < \alpha < 1$. The equilibrium plots show that the phase difference between the legs ranges from about 0 to $\frac{2\pi}{3}$ throughout a dig and that either left or right leg can lead.

The fact that such a large set of variations on the H functions yield similar behaviours is a very important result. The choice to use Morris-Lecar neurons itself was somewhat arbitrary, so it is necessary that the results be sufficiently robust to capture similar systems. Indeed, it may be more appropriate to model the network of *Emerita*'s CPGs by discussing their H functions rather that the neurons they might comprise. The results of this work suggest that certain systems of specific neurons can account for the observed behaviour. A much stronger suggestion is that, whatever the specific neurons involved, if $H(\phi)$ is qualitatively like $-\sin(\phi - \alpha)$, the network describes *Emerita*'s behaviour well. Conversely, if $H(\phi)$ is like $\sin(\phi - \alpha)$, then the

network fails to reproduce the behaviour.

Assuming that within the CPGs there are functional groups of neurons that give rise to the intrinsic CPG oscillations, the results of this study indicate that either inhibitory connections between like populations, or excitatory connections between unlike populations can initiate a phase difference between the fourth leg CPGs similar to that found in the data. This seems reasonable for the systems studied since exciting an unlike oscillator effectively inhibits a like one.

One final observation that has not received much attention is the fact that the frequency of the oscillation of each CPG diminishes as the dig progresses. Because, in these models, the oscillations are born by Hopf bifurcation, they can naturally assume a range of frequencies, so varying the parameter i_{app} is sufficient to account for the diminishing frequency of the CPGs throughout the dig. Imagine that there is a "dig" command or switch that generates a strong i_{app} initially, and that its intensity diminishes, resulting in a diminishing frequency for the Morris-Lecar oscillator. Of course, this explanation makes assumptions about the nature of the oscillators involved so it remains to be justified in future work.

The mechanism by which the bilateral coupling parameters a and b are attenuated remains to be explained, but it may actually be the result of sensory information about the organism's orientation, perhaps with respect to self-righting. The existing data show that either left leg or right leg can lead, and that during a dig, the leading leg can switch. This suggests that there may be a response linked to statocysts, or other sensory mechanisms that respond to orientation. Of course to test this hypothesis (or any other suggested by these models) would require lab time and, perhaps another thesis.

Bibliography

[1] G. B. Ermentrout and N. Kopell, *Frequency plateaus in a chain of weakly coupled oscillators, I*, Siam J. Math. Anal. **15** (1984), 215-237

[2] G. B. Ermentrout and N. Kopell, *Multiple pulse interactions and averaging in systems of coupled neural oscillators*, J. Math. Biol. **29** (1991), 195-217

[3] Z. Faulkes and D. H. Paul, *Digging in sand crabs (Decapoda, Anomura, Hippoidea): interleg coordination*, The Journal of Experimental Biology **200** (1997), 793-805

[4] Z. Faulkes and D. H. Paul, *Coordination between the legs and tail during digging and swimming in sand crabs*, J. Comp. Physiol. A **180** (1997), 161-169

[5] Z. Faulkes and D. H. Paul, *Digging in sand crabs: coordination of joints in individual legs*, The Journal of Experimental Biology **201** (1998), 2139-2149

[6] N. Fenichel, *Persistence and smoothness of invariant manifolds for flows*, Indiana University Mathematics Journal **21** (1971), 193-226

[7] M. Golubitsky and D. G. Schaeffer, *Singularities and Groups in Bifurcation Theory*, Springer, New York, 1985

[8] M. Golubitsky and I. Stewart, *Hopf Bifurcation in the presence of symmetry*, Arch. Rational Mech. Anal. **87** (1985), 107-165

[9] M. Golubitsky and I. Stewart, *Hopf bifurcation with dihedral group symmetry: coupled nonlinear oscillators*, Contemporary Mathematics **56** (1986), 131-173

[10] M. Golubitsky, I. Stewart and D. G. Schaeffer, *Singularities and Groups in Bifurcation Theory, vol 2.*, Springer, New York, 1985

[11] J. Guckenheimer and P. Holmes, *Nonlinear Oscillations, Dynamical Systems and Bifurcations of Vector Fields*, Springer, 1997

[12] A. L. Hodgkin and A. F. Huxley, *A qantitative description of membrane current and its application to conduction and excitation in nerve*, J. Physiol. **117** (1952), 500-544

[13] F. C. Hoppensteadt and E. M. Izhikevich, *Weakly Connected Neural Networks*, Springer, New York, 1997

[14] E. M. Izhikevich, *Phase equations for relaxation oscillators*, Siam J. Appl. Math **60** (2000), 1789-1805

[15] E. R. Kandel, J. H. Schwartz and T. M. Jessel, *Principles of Neuroscience*, Third ed., Elsevier, New York, 1991

[16] J. Keener and J. Sneyd, *Mathematical Physiology*, Springer, New York, 1998

[17] N. Kopell and G. B. Ermentrout, *Symmetry and phaselocking in chains of weakly coupled oscillators*, Communications on Pure and Applied Mathematics **49** (1986), 623-660

[18] N. Kopell and G. B. Ermentrout, *Phase transitions and other phenomena in chains of coupled oscillators*, Siam J. Appl. Math **50** (1990), 1014-1052

[19] N. Kopell, G. B. Ermentrout and T. L. Williams, *On chains of oscillators forced at one end*, Siam J. Appl. Math **51** (1991), 1397-1417

[20] C. Morris and H. Lecar, *Voltage oscillations in the barnacle giant muscle fiber*, Biophys. J. **35** (1981), 305-317.

[21] B. Mulloney and W. M. Hall, *Functional organization of crayfish abdominal ganglia III. Swimmeret motor neurons*, The Journal of Comparative Neurology **419** (2000), 233-243

[22] D. Murchison, A. Chrachiri and B. Mulloney, *A separate local pattern-generating circuit controls the movement of each swimmeret in crayfish*, J. Neurophysiol **70** (1993), 2620-2631

[23] D. H. Paul and B. Mulloney, *Local interneurons in the swimmeret system of the crayfish*, J. Comp Physiol A **156** (1985), 489-502

[24] D. H. Paul and B. Mulloney, *Nonspiking local interneuron in the motor pattern generator for the crayfish swimmeret*, J. Neurophysiol **54** (1985), 28-39

[25] D. H. Paul and B. Mulloney, *Intersegmental coordination of swimmeret rhythms in isolated nerve cords of crayfish*, J. Comp. Physiol A **158** (1986), 215-224

[26] V. Pearse, J. Pearse, M. Buchsbaum and R. Buchsbaum, *Living Invertebrates*, The Boxwood Press, California, 1987

[27] R. H. Rand and P. J. Holmes, *Bifurcation of periodic motions in two weakly coupled van der Pol oscillators*, J. Non-Linear Mechanics **15** (1980), 387-399

[28] F. K. Skinner, N. Kopell and E. Marder, *Mechanisms for oscillation and frequency control in reciprocally inhibitory model neural networks*, J. Comput. Neuroscience **1** (1994), 69-87

[29] F. K. Skinner, N. Kopell and B. Mulloney, *How does the crayfish swimmeret system work? Insights from nearest neighbour coupled oscillator models*, J. Comput. Neuroscience **4** (1997), 151-160

[30] F. K. Skinner, and B. Mulloney, *Intersegmental coordination of limb movements during locomotion: Mathematical models predict circuits that drive swimmeret beating*, The Journal of Neuroscience **18** (1998), 3831-3842

[31] F. K. Skinner, G. G. Turrigiano and E. Marder, *Frequency and burst duration in oscillating neurons and two cell networks*, Biol. Cybern. **69** (1993), 375-383

VITA

Surname: Hodge Given Names: Alexander Fraser Cooper

Place of Birth: Richmond, British Columbia, Canada

Educational Institutions Attended:

University of Victoria	1997 to 2003
University College of the Fraser Valley	1995 to 1997

Degrees Awarded:

B.Sc.	University of Victoria	2000

Honours and Awards:

Departmental Fellowship	2000 to 2002
Canwest Publishers Ltd. Scholarship	1996

Publications:

UNIVERSITY OF VICTORIA PARTIAL COPYRIGHT LICENCE

Title of Thesis:

Modeling Central Pattern Generators in Sand Crabs

Author 

Alexander Fraser Cooper Hodge

April 30, 2003